Synthesis of Ag-DLC coatings for biomedical implants

A Thesis Submitted to the

College of Graduate and Postdoctoral Studies

In Partial Fulfillment of the Requirements

For the Degree of Master of Science

In the Department of Mechanical Engineering

University of Saskatchewan

Saskatoon

Canada

By

Jaykumar Patel

PERMISSION TO USE

In presenting this thesis in partial fulfillment of the requirements for a Postgraduate degree from the University of Saskatchewan, I agree that the Libraries of this University may make it freely available for inspection. I further agree that permission for copying of this thesis in any manner, in whole or in part, for scholarly purposes may be granted by the professor who supervised my thesis work or, in their absence, by the College of Graduate and Postdoctoral Studies (CGPS), Head of the Department or the Dean of the College in which my thesis work was done. It is understood that any copying or publication or use of this thesis or parts thereof for financial gain shall not be allowed without my written permission. It is also understood that due recognition shall be given to me and to the University of Saskatchewan in any scholarly use which may be made of any material in my thesis/dissertation.

Requests for permission to copy or to make other uses of materials in this thesis/dissertation in whole or part should be addressed to:

Head of the Department of Mechanical Engineering
57 Campus Drive,
University of Saskatchewan
Saskatoon, Saskatchewan, S7N 5A9 Canada
OR
Dean
College of Graduate and Postdoctoral Studies
University of Saskatchewan
116 Thorvaldson Building, 110 Science Place
Saskatoon, Saskatchewan, S7N 5C9 Canada

ABSTRACT

The diamond-like carbon (DLC) coating has the potential to increase the lifetime of metal on polymer (MoP) type hip joints due to its good tribological and mechanical properties as well as excellent biocompatibility. However, the high internal compressive stress of DLC films limits their adhesion with CoCrMo alloy. The high internal stress can be minimized by doping the DLC coating with metals like Ti, Cu, W, Nb and many more.

In the present thesis work, silver (Ag) doped diamond-like carbon (DLC) coatings were prepared on the CoCrMo alloy using direct current (DC) magnetron sputtering for biomedical implants. The silver concentration was varied in the DLC matrix by varying the DC power to the silver target from 12 W to 18 W. Raman spectroscopy was carried out to evaluate the structural changes in the carbon matrix. X-ray photoelectron spectroscopy (XPS) was used to measure the concentration of Ag and sp^3 carbon hybridization in the coatings. The hardness, tribological behavior, and adhesion properties were characterized using nano-indentation, wear testing, and Rockwell C indentation, respectively. The hardness values show that initially, with a low percentage of silver, the residual stresses decrease drastically, whereas the hardness values decrease slightly. The lowest wear rate was observed for the coating doped with 7.4 at% of silver among all coatings, and improved adhesion was observed for all the Ag-DLC coating on CoCrMo alloy. The results showed that silver doped DLC coating is promising for a total hip joint replacement application.

ACKNOWLEDGEMENTS

First and foremost, I would like to thank my research supervisor, Dr. Qiaoqin Yang. Without her support and dedicated participation in every phase of the process, I might not be able to complete this research. I am very thankful for her support and understanding over the last two years.

I want to thank Professor Ikechukwuka Oguocha and Professor Duncan Cree, my committee members, for their helpful guidance. I want to thank Mr. Zhao Nan Fang and Mr. Robert Peace for their support, training, and patience. I am very grateful to Dr. Jason Maley at the Saskatchewan Structural Science Center (SSSC) for Raman spectroscopy training.

I highly appreciate the financial support granted by the Natural Sciences and Engineering Research Council of Canada (NSERC) and the University of Saskatchewan.

It took more than academic help to travel through my research, and I have many, numerous people to thank for tuning in and, on occasion, enduring me. I cannot begin to offer my appreciation and thanks for their companionship. Jesus Corona Gomez, Sheriff Adeniyi, and Mohamed Insaf Fariz have been unfaltering in their own and expert help during my time at the University.

Most significant, without my family, none of this could have happened. My mother gave her support every week by phone calls, despite my limited commitment to communications. For the last few years, my sisters have been kind and encouraging of me with their humor style. I also want to thank my sister, who opened both her home and heart when I first arrived in the city. This study stands as a testament to your unconditional love and support.

TABLE OF CONTENTS

LIST OF TABLES

LIST OF FIGURES

NOMENCLATURE

a-C	Hydrogen-free Amorphous Carbon
a-C:H	Hydrogenated Amorphous Carbon
Ag-DLC	Silver doped Diamond-like Carbon
BE	Binding Energy
CoC	Ceramic on Ceramic
CoP	Ceramic on Polymer
DLC	Diamond-like Carbon
E_d	Displacement Threshold
E_p	Penetration Threshold
FCVA	Filtered Cathodic Vacuum Arc
KE	Kinetic Energy
MoM	Metal on Metal
MoP	Metal on Polymer
MSIB	Mass-Selected Ion Beam
PEEK	Polyetheretherketone
PLD	Pulsed Laser Deposition
PTFE	Polytetrafluoroethylene
PVD	Physical Vapor Deposition
SCCM	Standard Cubic Centimeters per Minute
SEM	Scanning Electron Microscope
SSSC	Saskatchewan Structural Science Centre

Ta-C	Tetrahedral Hydrogen-free Carbon
Ta-C:H	Tetrahedral Hydrogenated Carbon
UHMWPE	Ultra-High Molecular Weight Polyethylene
UMT	Universal Mechanical Tester
XPS	X-ray Photoelectron Spectroscopy
γ	Surface Fracture Energy
σ_e	Extrinsic Stress
σ_i	Intrinsic Stress
σ_{th}	Thermal Stress

CHAPTER 1 – INTRODUCTION

1.1 Motivation

The joints in human bodies are made of bones and several related elements such as gristle, connective tissue, and nervous components. The joints fail when the cartilage cushioning between two bones wears out. The failure of the hip, knee, and spinal joints is increasing day by day due to the increased average weight and lifetime of human beings. The one way to overcome these issues is by using artificial joints. It is estimated that by 2030 the number of total hip replacements will rise by 572,000 (172%), and total knee replacements will increase by 3.48 million (673%) in the world [1]. The artificial joints are made of different bio-compatible alloys that can withstand the forces applied to joints. The most used alloys for artificial joints are stainless steel 316, titanium alloy, and cobalt alloy. These alloys' main problem is releasing toxic ions of the alloy elements after a lengthy application in the human body, which causes pain and damage the tissues. This problem would lead to a revision of expensive surgeries with a low success rate [2].

To overcome this problem, different surface modification techniques are being used. The most promising method is coating the prosthesis with hard thin coatings. Over the years, various coatings have been studied on the prosthesis. Diamond-like carbon (DLC) coatings have been shown to be the most promising ones because of their superior biocompatibility, high hardness, high corrosion resistance, low friction coefficient, and high wear resistance. However, DLC coatings have two drawbacks: (i) high internal/compressive stress and (ii) low adhesion to a metallic substrate. To withstand long-term wear resistance, the coatings should be thick (several micrometers) with good adhesion. However, it's difficult to obtain an adhesive

thick DLC coating on biomedical metals due to its high internal compressive stress: the coating will delaminate when the elastic energy per unit volume induced by the internal stress exceeds the surface fracture energy per unit surface area [3]. These drawbacks can be overcome by applying interlayers or doping [3–8].

1.2 Objectives

The overall objective of this thesis was to achieve DLC coatings on biomedical grade CoCrMo alloy with good adhesion and high wear resistance for biomedical applications by silver (Ag) doping. The specific objectives were:

- To achieve improved adhesion between DLC coating and CoCrMo alloy by Ag doping.
- To investigate the wear behavior of Ag-DLC coating on CoCrMo alloy.
- To achieve the lowest wear rate by optimizing Ag doping amount.

1.3 Research Contributions

1. Silver doped DLC (Ag-DLC) was successfully deposited on the CoCrMo alloy with enhanced adhesion for orthopedic applications.
2. Silver from Ag-DLC coating acts as a solid lubricant which reduces the wear rate of the ultra-high molecular weight polyethylene (UHMWPE).

The findings of this research would also help the researchers to understand the structure and the properties of silver doped non-hydrogenated diamond-like carbon coatings, which hold the great potential to be used in biomedical applications due to its improved wear coefficient for UHMWPE.

1.4 Thesis Organization

Chapter 1 introduces the motivation behind this research with objectives and contributions.

Chapter 2 covers the comprehensive review of CoCrMo alloy, carbon material, deposition techniques, the growth mechanism of the DLC coating, and working principles of different characterization techniques.

Chapter 3 covers the techniques and the conditions used to deposit the coating and to characterize it.

Chapter 4 presents the composition, structure, and mechanical properties of the silver doped coatings and discussed their relationships.

Chapter 5 summarizes the conclusions of this research and recommendations for future work.

CHAPTER 2 – LITERATURE REVIEW

The use of diamond-like carbon coating (DLC) for biomedical applications has attracted increasing attention due to its high hardness and low wear and corrosion rate. This chapter will provide a comprehensive review of artificial hip joints, CoCrMo alloy, diamond-like carbon coating, and its structure and characterization.

2.1 Artificial Hip Joints

Due to the relative motion in joints, the cartilage cushioning between two bones wears out and causes pain known as osteoarthritis. In this situation, the natural joints must be replaced by artificial hip joints. An artificial joint's lifetime depends on the material from which it is made and is usually less than 16 years.

Currently, four types of materials' configurations are being used in artificial hip joints: (i) metal on metal (MoM), (ii) metal on polymer (MoP), (iii) ceramic on ceramic (CoC), and (iv) ceramic on polymer (CoP).

Polytetrafluoroethylene (PTFE), Ultra-high molecular weight polyethylene (UHMWPE), or Polyetheretherketone (PEEK) are used to make acetabular cups in MoP or CoP. PTFE has a very high wear rate (0.5 mm per month) [9]. UHMWPE has been most widely used because many simple techniques such as irradiation and melting, irradiation and annealing, sequential irradiation with annealing can improve its wear rate by increasing its cross-linking [10].

Stainless steel, CoCrMo alloy, and Ti alloy are the most common metals for biomedical applications. Most MoM hip joints are made from CoCrMo alloy, and it can be divided into two categories: high carbon (>0.20 wt.%) and low carbon (<0.08 wt.%) [11]. Also, the alloys

can be manufactured by casting or forging. The cast alloy's grain size ranges from 30 µm to 1000 µm, whereas the forged alloy's grain size is less than 10 µm [12]. As mentioned above, the alloys have fair wear and corrosion resistance but release toxic ions into the body due to wear and corrosion. Coating it with non-toxic wear and corrosion-resistant materials becomes necessary to reduce the release of toxic ions from alloy.

Many different coatings have been investigated on CoCrMo alloy to increase the wear and corrosion resistance of total hip joint and to reduce the release of toxic ions. DLC coating is the most promising one due to its excellent biocompatibility and high wear and corrosion resistance [13].

2.1.1 Metal on Polymer type hip joints

The first metal on metal prosthesis was introduced by McKee and Farrar in the 1950s [10]. Over the years, many improvements took place in MoM type prosthesis to reduce its wear rate from 5 to 1 mm^3/year [10]. Nevertheless, the MoM prosthesis disappeared entirely from the market in the early 2000s due to toxic debris release. Since the mid-1990s, the metal on polymer type hip joints have been widely used for older and less active people due to their low cost, low wear rate of 0.1 mm^3/year, and high durability and high performance [10,14]. However, the release of toxic ions like Cr^{3+} and Cr^{6+} can damage liver , kidney, lungs and respiratory system [15]. The components of MoP type total hip joint is shown in Figure 2.1.

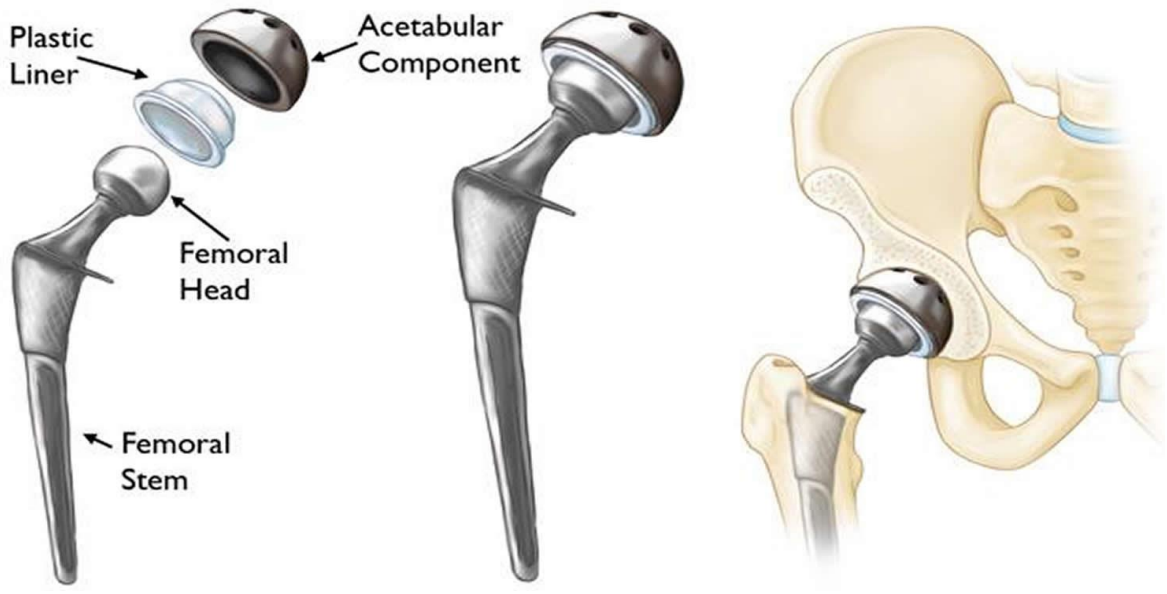

Figure 2.1. The components of total hip joint and its assembly [16].

The most important factor in metal on polymer type hip joints is the wear rate of polymer (UHMWPE), which reduces the performance and the life span of the hip joint. The released debris from the UHMWPE cause implant loosening, tissue damage and bone loss [17].

2.1.2 Overview of CoCrMo alloy

Elwood Haynes first introduced cobalt-chromium alloy in the early 1900s [18]. It showed high corrosion resistance because of the formation of dense Cr_2O_3 passive oxide coatings to prevent further corrosion [19]. Currently, many cobalt-chromium alloys are available in the market based on standards, like ASTM F-75 and ASTM F1537. ASTM F-75 is the one used for medical implants, and its composition is described in Table 2.1.

Table 2.1. Composition of ASTM F-75 CoCrMo alloy [20].

Element	Composition, % (Mass/Mass)	
	Minimum	Maximum
Chromium	27.00	30.00
Molybdenum	5.00	7.00
Nickel	-	0.50
Iron	-	0.75
Carbon	-	0.35
Silicon	-	1.00
Manganese	-	1.00
Tungsten	-	0.20
Phosphorous	-	0.02
Sulfur	-	0.01
Nitrogen	-	0.25
Aluminum	-	0.10
Titanium	-	0.10
Boron	-	0.01
Cobalt	63.71	58.71

2.1.3 Overview of UHMWPE

UHMWPE was introduced in 1962 by Charnley to overcome the drawbacks of PTFE [21]. This polymer's chemical formula is $(-C_2-H_4-)_n$, in which "n" indicates the degree of polymerization. According to the ASTM D6712-17 standard, the minimum degree of polymerization should be 36,000 [22]. UHMWPE's wear in an artificial hip joint is mainly

caused by two mechanisms: (i) abrasive wear and (ii) adhesive wear, which produces UHMWPE fibers in MoP hip joints. Reducing roughness and increasing hardness are the two ways to decrease its adhesive/abrasive wear rate. Many techniques, including irradiation and melting, irradiation and annealing, sequential irradiation with annealing, were used to increase its hardness for lowering its wear rate [10].

2.2 Carbon materials

Carbon is a chemical element with an atomic number of 6, and one atom has four valance electrons available to form covalent bonds with other atoms. It is the fourth most common element in the universe and the fifteenth-most found material in the earth's crust [23]. Also, carbon is the main component of the human body, with a mass concentration of 18.5% [23]. Its four valance electrons can be hybridized to either sp^3, or sp^2, or sp^1, making it feasible to form different crystalline and disordered structures.

2.2.1 Hybridization of carbon

Hybridization is the concept of mixing atomic orbitals into new hybrid orbitals with different energies and shapes [24]. For carbon, two valance electrons are in 2s orbit, and another two electrons are in 2p orbit. In an excited state, an electron from the 2s orbit can move into the 2p orbit.

As shown in Figure 2.2, in sp^3 hybridization, three p orbitals and one s orbital are combined to create four hybrid orbitals. The energy level of sp^3 orbitals is close to that of 2p because the sp^3 hybrid orbitals are of 75% p orbital character. sp^3 hybridized carbon orbitals form a tetrahedral structure with an angle of 109.5^o.

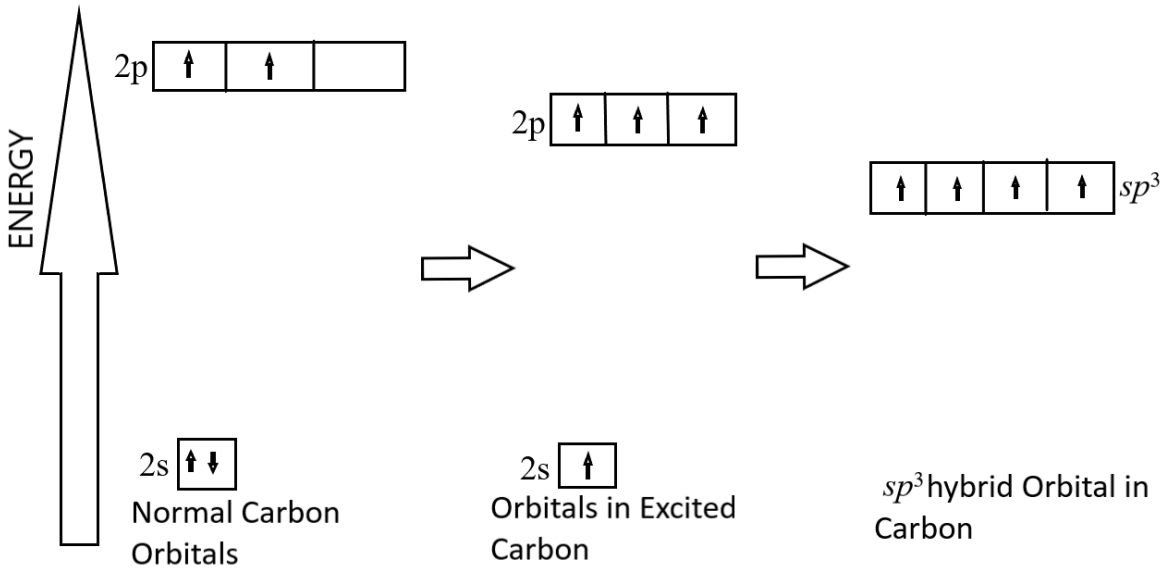

Figure 2.2. sp^3 hybridization in carbon.

As shown in Figure 2.3, in sp^2 hybridization, two p orbitals and one s orbital are combined to create three hybrid orbitals. The energy level of sp^2 orbitals is lower than that of sp^3 orbitals because the sp^2 hybrid orbitals are 66.7% of p character, less than that in sp^3 orbitals. sp^2 hybridized carbon orbitals form a trigonal planer structure with an angle of 120^{o,} and an unhybridized p orbital lies perpendicular to the trigonal plane.

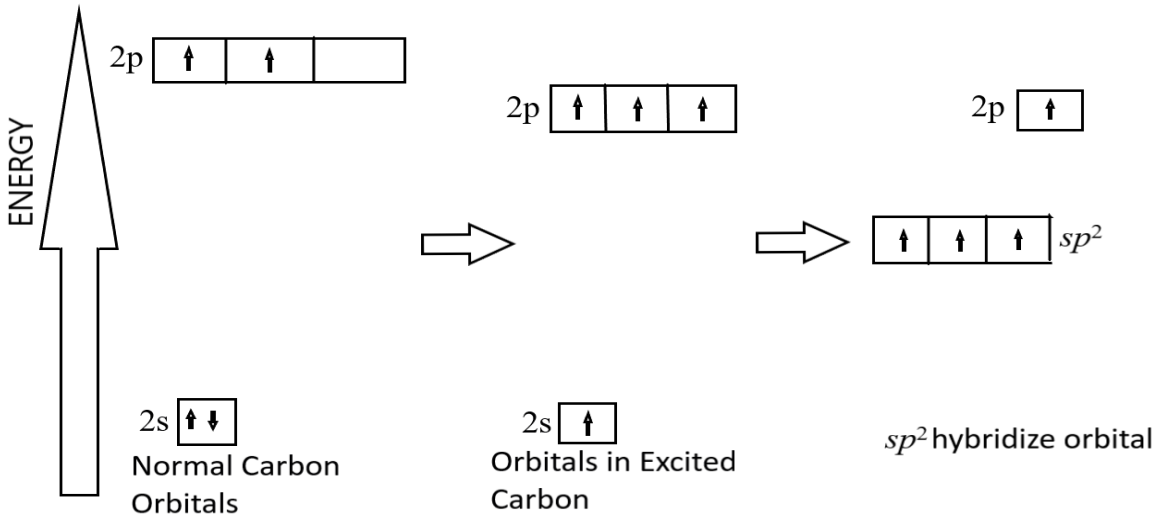

Figure 2.3. sp^2 hybridizations in carbon.

As shown in Figure 2.4, in *sp* hybridization, one p orbital and one s orbital are combined to create two hybrid orbitals. The *sp* orbitals' energy level is between 2s and 2p orbitals because the *sp* hybrid orbital is 50% p character. *Sp* hybridized carbon orbitals form a linear structure with an angle of 180^{o}.

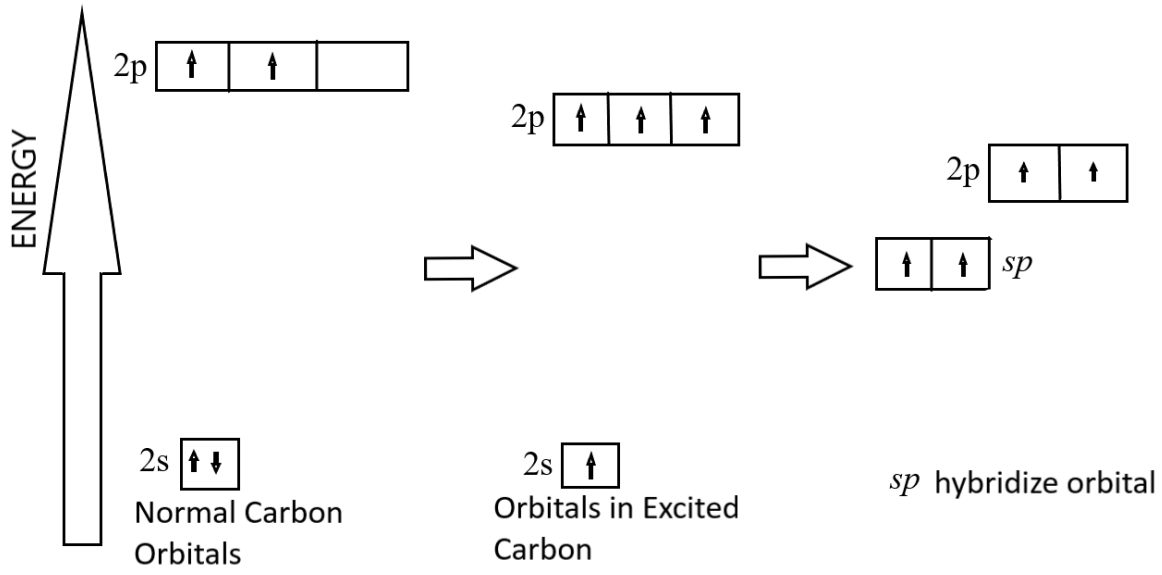

Figure 2.4. *sp* hybridization in carbon.

2.3 DLC thin coatings

The first amorphous carbon coating was reported in 1953 by Heinz Schmellenmeier [25]. In the early 1970s, Eisenberg and Chabot deposited DLC thin coatings using dual ion beams on a negatively biased metallic substrate [26]. DLC thin coatings can be divided into hydrogen-free amorphous carbon (a-C), tetrahedral hydrogen-free carbon (ta-C), hydrogenated amorphous carbon (a-C: H), and tetrahedral hydrogenated amorphous carbon (ta-C: H). The properties of different amorphous carbon coatings are summarized in Table 2.2.

Table 2.2. Properties of different amorphous carbon coatings [27–29].

Material	sp^3 (%)	H (%)	Density ($g/cm^{3)}$	Hardness (GPa)
a-C	5	0	2.2	
Ta-C	80 - 88	0	3.1	80
a-C:H	40 - 60	30 - 50	1.2 - 2.2	10 - 20
Ta-C:H	70	30	2.4	50

2.3.1 Deposition techniques and formation mechanism

DLC can be deposited using various techniques like ion beam, sputtering, cathodic arc, pulsed laser deposition (PLD), and plasma-enhanced chemical vapor deposition. The deposition technique can be selected according to the structure and property needed in the coating.

As shown in Figure 2.5, the carbon ions are created from the graphite cathode in the ion-beam deposition. The ionized carbon ions are accelerated to form an ion beam in a vacuum. There are different ion beam deposition variants, including the cascade arc source and mass-selected ion beam (MSIB). In MSIB, the carbon ion species with a well-defined energy level were produced for deposition: the equipment is expensive. The deposition rate is low and is thus mainly used for research in laboratories.

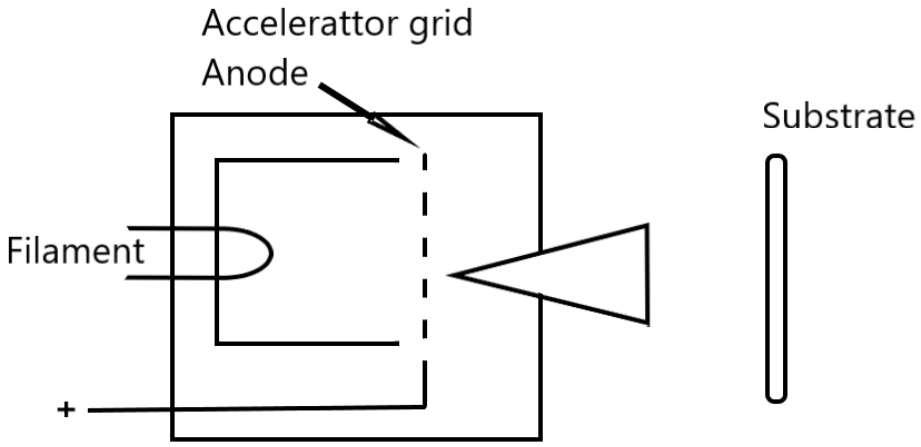

Figure 2.5. Schematic of ion beam deposition.

Another method to deposit DLC is a cathodic arc, which is widely used in industries shown in Figure 2.6. Inside the vacuum chamber, the arc is created using a carbon electrode (striker) and graphite target as a cathode. The low voltage and high current in the arc can easily create plasma with high ion density. The plasma ions can be filtered using the toroidal magnetic filter. In this case, it is known as a filtered cathodic vacuum arc (FCVA). FCVA narrows down the ion energy distribution, promoting the deposition rate and lowering the cost.

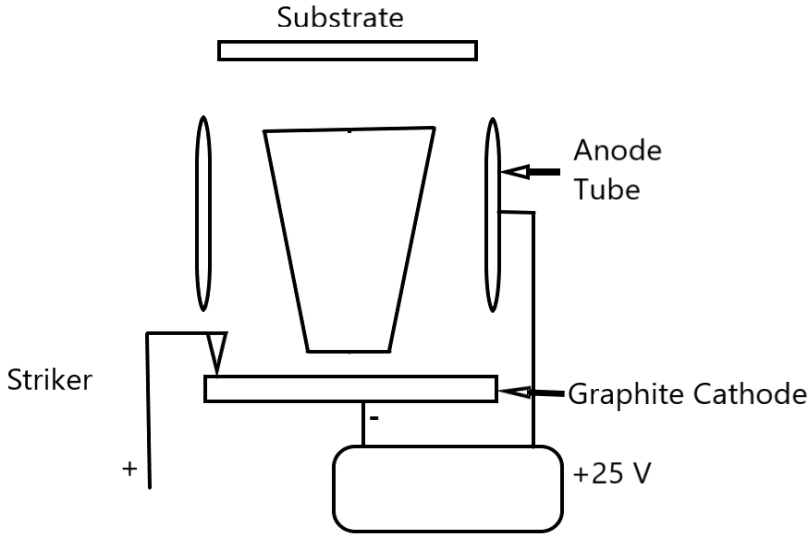

Figure 2.6. Schematic of filtered cathodic vacuum arc.

Sputtering is the most widely used industrial process for DLC deposition [3,26–28]. In a sputtering deposition system, any material can be the target to be sputtered off to form a thin coating on the substrate, and the system can be scaled up easily. The schematic diagram of sputtering deposition is shown in Figure 2.7. For DLC deposition, graphite is usually used as the target. As graphite has a low sputtering yield, magnetron sputtering is generally used. In a magnetron sputtering system, the magnets are placed behind the target to increase the path length of argon ions, which increases the degree of ionization of plasma [3]. Ion beam sputtering is also used for well-controlled DLC deposition.

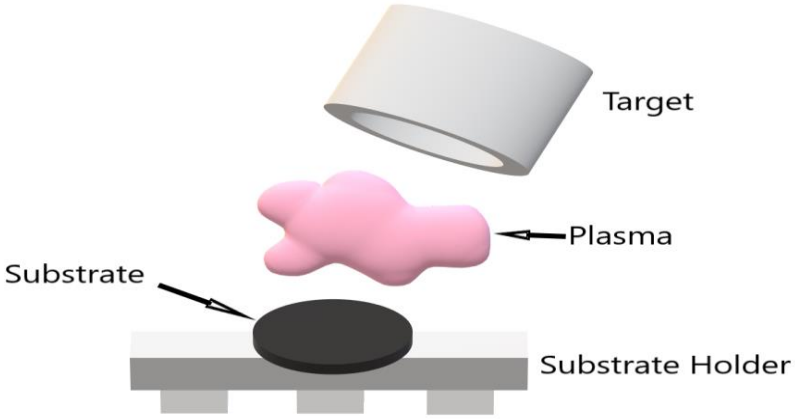

Figure 2.7. Schematic of sputtering deposition.

Many researchers attempted to understand DLC's deposition mechanism and proposed a few different models [32–34]. The most recent one was explained by Robertson et al. [3,27,28] as follows: At the penetration threshold E_p, the ions can penetrate the surface layer. The energy required to move the atom is the displacement threshold, E_d. The surface binding energy equals the sublimation energy or cohesive energy, or 7.4 eV for carbon. Therefore, E_d of 25 eV gives E_p = 32 eV [3,27,28].

When carbon ions with low energy bombard an amorphous carbon surface, they cannot penetrate the surface and stick on the surface in the sp^2 state. The ions with energy higher than the penetration threshold E_p can penetrate the surface, which will increase the local density. If the ion energy increases further, more energy will be used to displace the atoms. The remaining energy must be dissipated from the ions in the form of phonons, which will reduce the density.

2.3.2 Stresses in coatings

Many applications, especially protective applications, require coatings with a thickness of several micrometers. However, the maximum coating thickness without delamination is determined by the stresses in the coating. A coating of thickness T will delaminate when the elastic energy per unit volume due to the stress σ exceeds the surface fracture energy γ per unit surface [3].

$$2\gamma > \frac{\sigma^2 T}{2E} \text{ or } T < \frac{4\gamma E}{\sigma^2} \quad (2.1)$$

The residual stress is a combination of thermal stress (σ_{th}), intrinsic stress (σ_i), and extrinsic stress (σ_e).

$$\sigma = \sigma_{th} + \sigma_i + \sigma_e \quad (2.2)$$

Thermal stresses arise from the difference in the thermal coefficient of expansion of substrate(α_s) and coating(α_f) material $(\alpha_s) - (\alpha_f)$ with the combination of temperature difference $(T_r - T_d)$ [35]. The thermal stress can be calculated from equation (2.3), where E_f is Young's modulus, and V_f is Poisson's ratio.

$$\sigma_{th} = \left(\frac{E_f}{1 - v_f}\right)(\alpha_s - \alpha_f)(T_r - T_d) \quad (2.3)$$

Intrinsic stresses arise during the deposition, which can be tensile stress or compressive stress. The tensile stress is produced in the coating from the non-energetic particles that cannot

fill the voids and create coating vacancies [35]. As the energy of incident particles increases, it can penetrate the surface and fill the vacancies and voids (grain boundary spacing and intercolumnar space) [35]. Further increase in the energy of incident particles will increase the compressive stress [35].

Extrinsic stresses arise from the interaction of coating and the atmosphere. A lattice distortion may originate from various sources, such as the incorporation of impurities [35].

2.3.3 Wear mechanism in DLC coated hip joint

In general, wear mechanisms include abrasive, adhesive, fatigue, erosive, corrosive, and impact wear, depending on the contact modes (sliding, rolling, mixed rolling and sliding, impact, and mixed impact sliding) of surfaces.

Abrasive wear takes place when the hard particles are forced against surfaces. It can happen in three different mechanisms: plowing, cutting, and fragmentation [36]. Plowing occurs when the material is plastically deformed and forms grooves. Cutting occurs when the portion of the material is separated from the surface. When the cutting process creates a crack on the surface, the crack will propagate around the grooves to fragmentation. Due to the high hardness and high strain tolerance of the DLC surface, abrasive wear would not occur on the DLC surface but on the polymer counter surface and leave debris between two the surfaces [36].

Adhesive wear is found between the two moving surfaces in contact with friction. In this case, plastic deformation occurs during relative motion, creating debris and transferring it from one surface to another. The produced debris may cause abrasive wear on the softer surface. In the case of DLC coating sliding with polymer, carbon-based tribo-film would form on the polymer surface, reducing the coefficient of friction [36].When cyclic loading between two surfaces exceeds one of the surfaces' fatigue limits, material particles will be removed from

the surface. The released particles will increase abrasive wear and adhesive wear by increasing the friction between two surfaces. The fatigue limit generally decreases with increasing the ratio of hardness to the elastic modulus.

Tiainen et al. and Lappalainen et al. measure the wear performance of tetrahedral amorphous carbon-coated metal hip joint against UHMWPE in 1 wt% aq NaCl medium using ball–on-disc tester and found a reduction of wear rate of UHMWPE by a factor of 10, compared to the uncoated sample [37,38]. Oate et al. evaluated the wear performance of DLC coated CoCrMo alloy against UHMWPE cup in knee simulator using water as a lubricant and found a reduction of wear rate of UHMWPE by a factor of 5 [39].

2.4 Metal doped DLC (Me-DLC) thin coatings

DLC thin coatings can be alloyed or doped with different elements to improve their properties like hardness, biocompatibility, electric conductivity, wear resistance while maintaining their diamond-like amorphous nature.

There are two ways to reduce the stress of DLC coatings and increase their adhesion. One way is to deposit a thin layer of a good carbide former like W or Cr before DLC's deposition [6,34–36]. Another way is to dope the DLC coatings with metals [43–47]. Doping can increase adhesion but increase or decrease other properties like hardness and toughness depending on the doping element and its concentration. The doped elements can exist in carbide form or nanocrystalline elemental form inside the coating. Improved adhesion of DLC was found on many types of steels by incorporating silicon, chromium, or titanium [17]. For industrial applications, graded coatings with better adhesion were widely used. In graded coatings, the chemical and the mechanical properties are gradually changed from substrate material to pure

metal layer and then to metal doped DLC layer and pure DLC layer on the top surface. The metal atoms may be dissolved into DLC matrix at a low concentration and form clusters inside DLC matrix at higher concentrations [31]. For tribological application, DLC was generally doped with carbide forming elements of group IVa V, or Via [31]. For biomedical applications, the dopant should be non-toxic to the human body.

Most researchers focused on using doping elements to form carbide in the DLC coatings to enhance the coating's hardness. Nevertheless, non- carbide former like silver (Ag) was also used as a dopant for DLC coatings. Because of its low dissolvability and inactivity to carbon [48], silver isolates as an optional stage in the carbon framework. These sorts of nano-groups are usually found in comparable coatings doped by low dissolvable metal components. Manninen et al. [49] deposited Ag-doped DLC (Ag-DLC) on SS316 using magnetron sputtering and found no change in hardness and wear rate for Ag content up to 6.7 at% in DLC. Wu et al. [50] deposited Ag-DLC with 3.55 at% of Ag on stainless steel using magnetron sputtering in an Ar-CH_4 mixture and found a remarkable drop in internal stress and friction coefficient, but there was no change in hardness. However, Pisarik et al. [5] deposited Ag-DLC on titanium alloy using a dual PLD technique. They found a gradual increase in toughness as the doped amount of Ag increased from 0 at% to 10 at%. Mazare et al. [51] deposited Ag-DLC on titanium using a thermionic vacuum arc process. They found that the particle size of Ag increased with the increase of Ag concentration in the coating. A similar result was noticed by Wu et al. [50]. It was due to Ag's tendency to form clusters on or near the surface during the deposition. It has been found that the maximum Ag concentration doped in the coating without any side effects to the human tissues was 10 at% [4,6,51,52].

2.5 Non-destructive characterization of Me-DLC coatings

2.5.1 Raman spectroscopy

Raman spectroscopy is a powerful approach to characterize the bonding states of DLC coatings. Raman spectroscopy is based on the scattering of the photons from the laser. When the photon is absorbed or interacts with the atom, another photon with different energy is emitted, known as scattering. Scattering can be classified as elastic scattering and inelastic scattering.

Elastic or coherent scattering occurs when there is no change in the incident's energy and emitted photons, known as Rayleigh scattering. Inelastic or incoherent scattering happened when there is a change in the incident's energy and emitted photons. Most light is Rayleigh scattered, and Raman scattering occurs once in 10 million photons. While photons and molecular vibration are exchanged during the interaction, if photons lose the energy, it is known as stokes. If photons gain energy, then it is known as anti-stokes.

The output results are plotted as the intensity of scattered light vs. each frequency of light. The Raman active modes for DLC include disordered D peak at 1350 cm^{-1} and graphitic peak G peak at 1580 cm^{-1}. The typical Raman spectra of different carbon materials are shown in Figure 2.8.

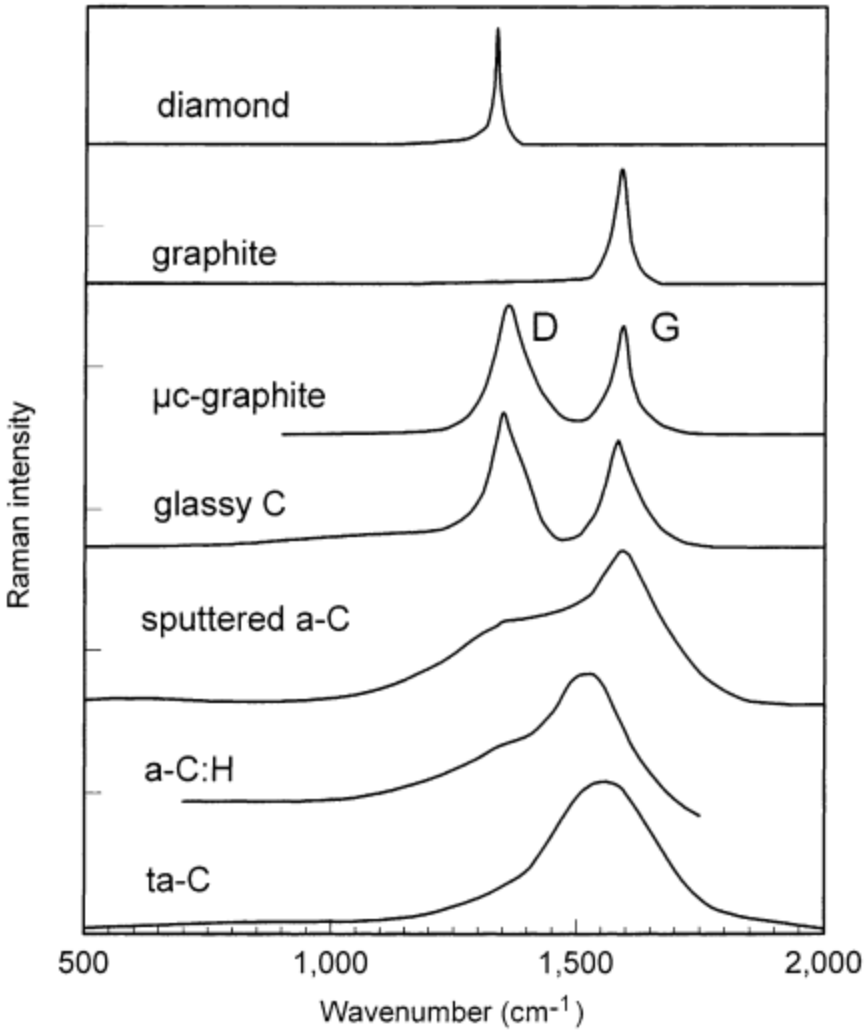

Figure 2.8. Comparison of Raman spectra for different carbon materials [3].

The G peak is due to the bond stretching of sp^2 carbon in chain and ring structure and always present in all types of carbon coating[53]. The D peak is a result of breathing modes of sp^2 bonds in ring structure [53] and the size of sp^2 phase organized in rings can be determined from the I(D)/I(G) ratio in amorphous carbon thin films [54].

2.5.2 X-ray photoelectron spectroscopy

X-ray photoelectron spectroscopy (XPS) is widely used to characterize the surface's elemental composition and bonding states. In XPS, monoenergetic soft X-rays interact with the atoms of the sample surface, as shown in Figure 2.9. If the photon's energy is sufficiently high, it will result in the electron's emission from the atoms' inner shells. The kinetic energy (KE) that remains on the emitted electrons is measured [55]. This kinetic energy is useful since this is discrete and is a function of the electron binding energy (BE), which, in turn, is specific to an element and its environment [55].

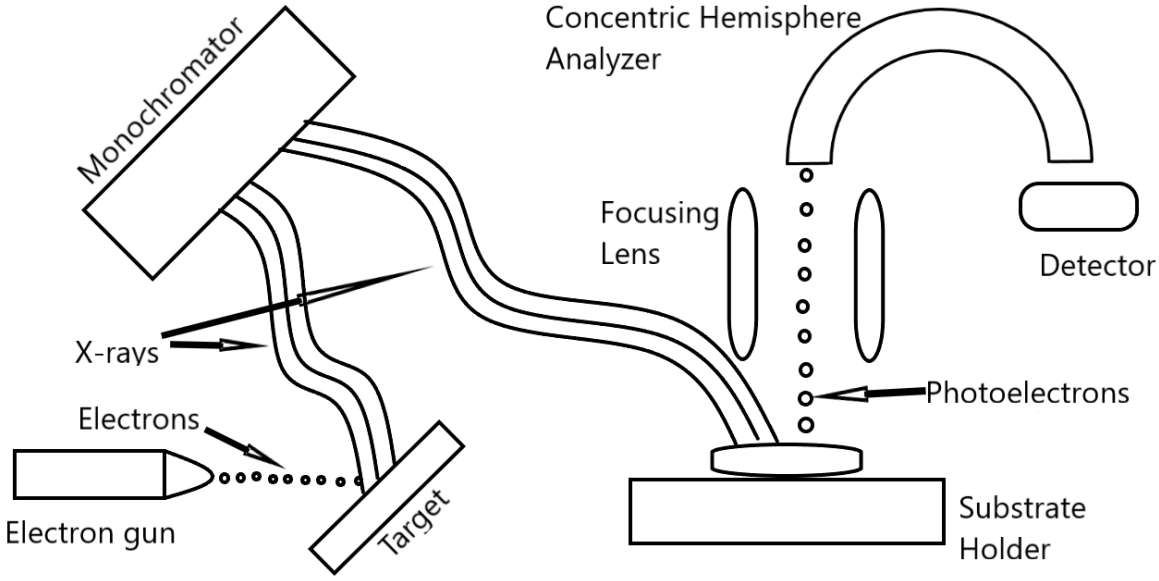

Figure 2.9. Schematic diagram of XPS.

XPS can also be used to map the distribution of emitted electrons representing the distribution of specific element on surface [55]. There are two approaches to map the elements based on the collected signals.

Serial mapping collects the data point by point and reconstruct it in pixel by pixel. In this case, the spatial resolution depends on the smallest area that can be analyzed. In parallel

mapping, electron emission from the whole area is detected by a 2D detector without scanning. Then the detector sort out the electron emission within preselected kinetic energy.

2.6 Mechanical characterization of carbon coatings

2.6.1 Adhesion

There are a few techniques to evaluate the adhesion of coatings to the substrate. Pull-off testing is used to measure low adhesion coating, usually on a polymer substrate. Scratch testing is designed to measure high adhesion coating quantitatively. The Rockwell-C (VDI 3198) indentation is to evaluate the coatings adhesion strength qualitatively.

In the Rockwell-C indentation method, a normal load of 1471 N is applied to the coating's surface, and the indentation and its surrounding area are then observed with a microscope. The level of delamination and crack formation around the circular perimeter of the indentation is compared with a well-established adhesion quality guideline known as VDI(The association of German engineers) guidelines 3198 [56]. As shown in Figure 2.10, some microcracks or short microcracks combined with a small amount of delamination around the indentation area indicate good adhesion, whereas severe delamination around the indent's circumference is an unacceptable failure, meaning poor adhesion.

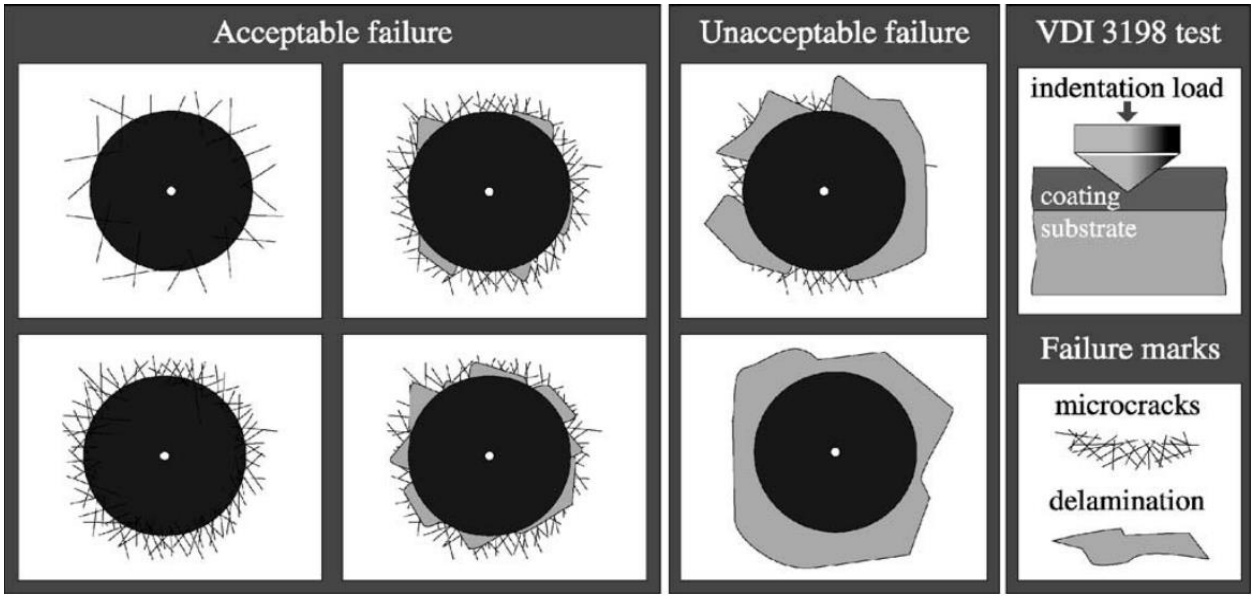

Figure 2.10. The principle of the VDI 3198 indentation test [56].

2.6.2 Hardness

Hardness is the ability of the material to resisting plastic deformation. Indentation techniques are used to measure the hardness. A hard tip is being pushed into the sample's surface, and the hardness is described as the ratio of the load applied to the plastically deformed area of the sample. In micro indentation techniques, the load ranging from 100 mN to several N is used. In this case, the elastic behavior cannot be measured, and the measured hardness may be affected by the substrate for thin coatings.

Recently developed nano-indentation can solve both issues. In nano-indentation, an apparatus applies load as low as several nano newtons, measures the displacement, and uses an indenter tip with a calibrated area function. One can then use the load-displacement curves to obtain both the hardness and elastic modulus.

The thickness of the thin coating is a critical factor in measuring the hardness. If the indentation depth is more than 1/10 of the coating thickness, the underlying substrate will

influence the test results. To avoid the substrate's effect, the coating thickness must be at least ten times the indentation depth or six times greater than the indentation radius, whichever is greater [57].

2.6.3 Wear

Wear is a loss of a material due to moving contact with other surfaces, and friction is caused by two surfaces' relative motion in contact. The friction coefficient describes the ratio of friction force to the applied normal load. Friction and wear are not a fundamental property of material because it depends on the environment and the testing conditions. There are different testing configurations to measure friction and wear.

Wear can be measured either as a weight loss or as a volume loss. Since the tribological testing results are affected by the testing conditions, the wear tests are designed to simulate the application conditions. Figure 2.11 shows the schematic diagram of a typical pin-on-disc wear tester used in this work.

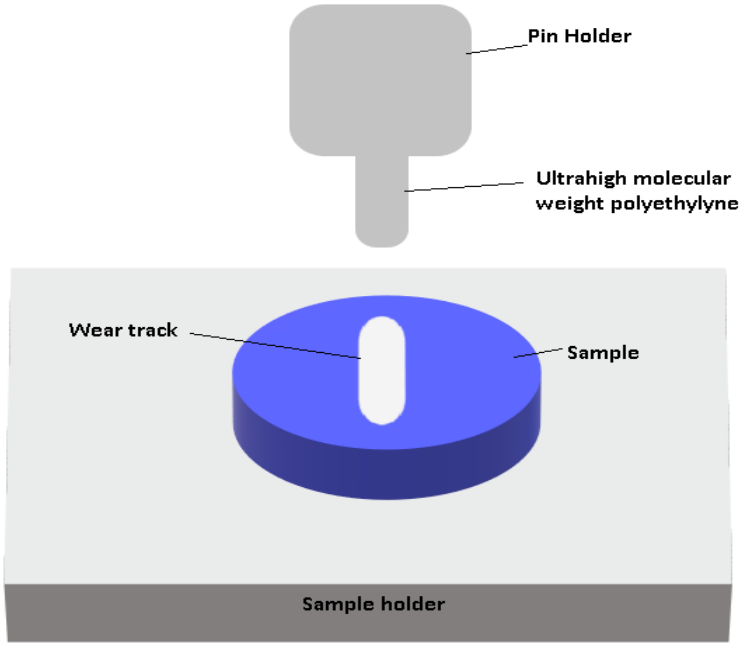

Figure 2.11. Schematic diagram of a typical pin-on-disc wear tester.

CHAPTER 3 – MATERIALS AND METHODS

In the present study, physical vapor deposition (PVD) (magnetron sputtering) was used to deposit silver doped diamond-like carbon (Ag-DLC) coatings. DC power source was used to sputter the graphite target, and pulsed DC was used to sputter the silver target. After the deposition, the coatings' hardness and elastic modulus were measured using nano-indentation, and their tribological behavior was evaluated using a pin-on-disk wear tester. Their structural characteristics were analyzed using Raman spectroscopy and X-ray photoelectron spectroscopy. The detailed procedures of all the techniques are described in the following sections.

3.1 Thin coating deposition

3.1.1 Sample preparation

The CoCrMo alloy samples with a size of 25.4 mm in diameter were ground and then polished using silicon carbide abrasive papers and diamond particles with sizes of 9 µm, 3 µm, and 1 µm, sequentially. The polished CoCrMo alloy sample is shown in Figure 3.1. After polishing, the samples were cleaned ultrasonically in acetone for 20 minutes.

Figure 3.1. Polished CoCrMo alloy.

Before thin coating deposition, the samples were argon cleaned in the PVD system for one hour. The parameters used for Ar cleaning are listed in Table 3.1.

Table 3.1. Parameter for Ar cleaning.

Ar flow Rate (sccm)	Working Pressure (* 10^{-6} Torr)	Substrate Bias (Watts)	Working Distance (mm)	Rotation of Substrate (RPM)
30	10	50	60	3

3.1.2 Physical vapor deposition system

The PVD system, model: SPT320 sputtering system, manufactured by Plasmionique Inc., was used to deposit Ag-DLC coatings. The system is equipped with three magnetrons, a plasma source, a rotating substrate holder, a vacuum chamber, a load lock chamber, and a pumping system. The schematic diagram of the PVD system is shown in Figure 3.2.

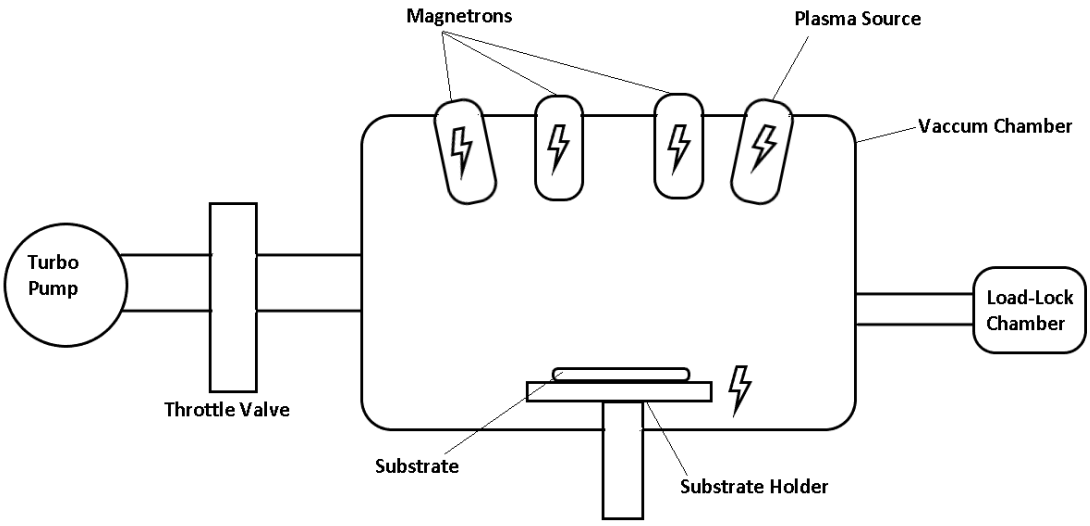

Figure 3.2. Schematic diagram of the PVD system.

The PVD system is equipped with three radio frequency (RF) (one for magnetron sputtering, another one for generating plasma, and the other one for substrate biasing) and two DC power sources (one for sputtering graphite and the other one for sputtering Ag). Their power limits are shown in Table 3.2.

Table 3.2. Power limit of different components.

Component	**Maximum RF power**	**Maximum DC power**
Magnetron 1	150 W	300 W
Magnetron 2	150 W	300 W
Magnetron 3	150 W	300 W
Plasma Source	250 W	N/A
Substrate Bias	150 W	N/A

For DLC coating deposition, the inert argon (Ar) gas was used as the ion source for sputtering, and the graphite target was used as a carbon precursor. During the deposition, the DC power of 300 W was applied to the graphite target to accelerate the Ar ions. The bombardment of Ar ions evaporates the graphite target by transferring the momentum. Simultaneously, a pulsed DC source with different powers was supplied to the silver target to evaporate Ag. A negative bias of 162 V (50 W) was applied to the substrate holder to accelerate the Ar, carbon, and Ag ions towards the substrate. The sputtered carbon and Ag atoms combined with carbon and Ag ions with high kinetic energy were then condensed onto the substrate to form Ag-DLC coatings described in section 2.3.1. The silver target's power was varied from 12 W (the minimum power required to sputter the silver) to 18 W, where the

silver's concentration in the coating exceeds 10 at%. The deposition parameters for depositing Ag-DLC coatings are summarized in Table 3.3.

Table 3.3 Parameters used for deposition of Ag-DLC coatings.

Coating	Pressure (* 10^{-6}) Torr	Substrate Temperature (^{o}C)	Power to Graphite (DC Continuous)	Power to Silver (Pulsed DC)	Power to Substrate	Power to the Plasma Source
DLC	10	25	300 W	0 W	50 W	200 W
Ag-DLC-1	10	26	300 W	12 W	50 W	200 W
Ag-DLC-2	10	30	300 W	14 W	50 W	200 W
Ag-DLC-3	10	28	300 W	16 W	50 W	200 W
Ag-DLC-4	10	29	300 W	18 W	50 W	200 W

The substrate temperature was maintained at ambient temperature during the deposition using a cooling system. The deposition time was 3 hours for all the samples, and the working distance (60 mm), substrate rotation (3 RPM), and Ar flow rate (30 sccm) were kept constant for all the sample depositions.

3.2 Structural Characterization

3.2.1 Raman Spectroscopy

Raman spectroscope (Reinshaw 2000) at Saskatchewan Structural Science Centre (SSSC) was used to characterize the coatings' structure. Ar ion laser with a wavelength of 514.5 nm was used as the light source. A 50X objective lens with 100% power was used to take Raman spectra. The head power was 10 mW, and the power at the spot on the sample was 2.74 mW. Before every test, internal calibration was carried out using a silicon standard. Each test was performed for an exposure time of 10 seconds to avoid the burning of the samples, and ten

accumulations were done to reduce the noise. The schematic diagram of the Raman Spectroscope is shown in Figure 3.3.

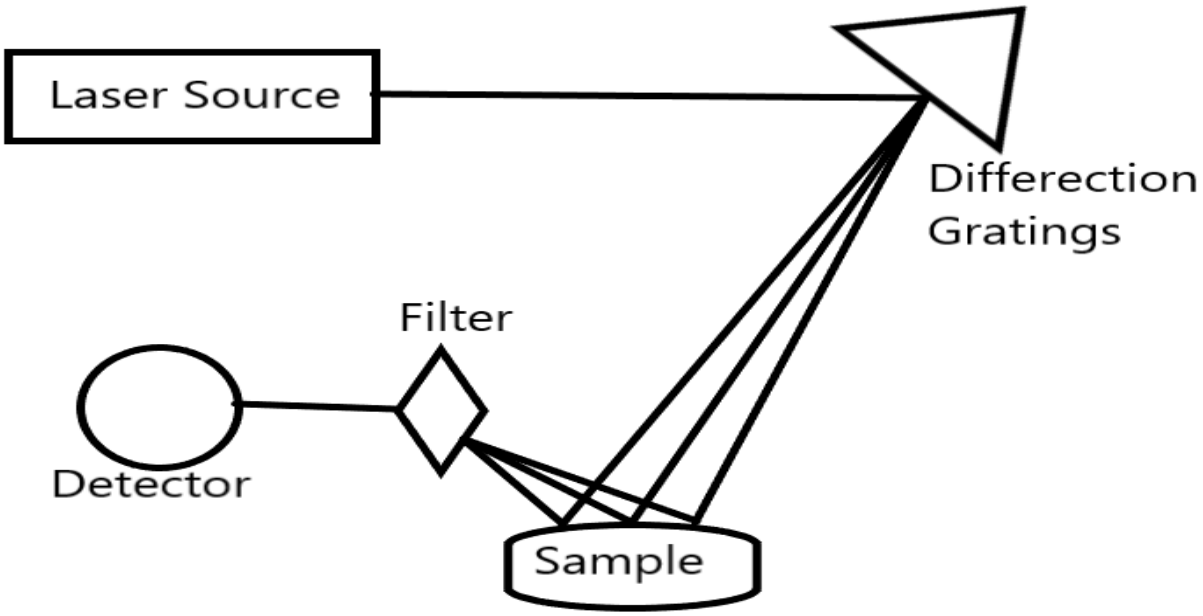

Figure 3.3. Schematic diagram of a Raman spectrometer.

3.2.2 X-ray photoelectron spectroscopy (XPS)

XPS measurements were carried out using Kratos AXIS Supra at SSSC. The 500 mm Rowland circle monochromatic Al K-α (1486.6 eV) source was used with a spot size of 300 X 700 microns. All survey scan spectra were collected in the binding energy range of 0 eV to 1275 eV with a pass energy of 160 eV and 1 eV step. For high-resolution scans, pass energy of 20 eV and a step of 0.05 eV were used.

3.2.3 Surface topography and morphology

Zygo NewView 8000 at the College of Engineering was used for surface topography observation and coating thickness measurement. For thickness measurement, it was assumed the optical thickness is the same as the geometric thickness, and the DLC coatings are transparent.

Joel JSM-6010LV scanning electron microscope (SEM) at the College of Engineering was used to observe the level of cracks and delamination of the Rockwell C indents and their surrounding area.

3.3 Mechanical Characterization

3.3.1 Nano-indentation

The nano head equipped on the Universal Mechanical Tester (UMT) was used to carry out nano-indentation. Berkovich indenter tip of 100 nm was placed perpendicular to the surface and pushed into the surface by a gradual increase in the load up to a set value and kept 60 seconds to eliminate the effect of material's creep. After that, the load was gradually removed.

For each sample, 50 indents were carried out in the form of a 5 X 10 matrix. Initially, the load was varied from 1 mN to 6 mN, and then 3 mN was selected for all the indents since the indentation depth for 3 mN was less than 10% of the coating thickness.

3.3.2 Rockwell C indentation

Rockwell C indentation was used to evaluate the adhesion of Ag-DLC coatings on CoCrMo alloy qualitatively. A load of 1471 N was applied according to the VDI 3198 standard [56]. Three different indents were done on each sample and then observed using SEM for spallation

and cracks at the imprint and surrounding area. The details regarding the standard VDI3198 have been described in section 2.6.1.

3.3.3 Wear tests

The wear tests were carried out using a pin-on-disc tester equipped with an universal materials tester from CETR. A circular (4.5 mm diameter) flat-ended pin of ultrahigh molecular weight polyethylene (UHMWPE) was used as a counterpart in the pin-on-disk configuration described in section 2.6.3. The tests were conducted in distilled water at room temperature. A constant normal load of 10 N was applied for 10000 cycles. The sliding distance was 12.5 mm, and the sliding speed was 25 mm/sec. The volume and the weight of the UHMWPE pins and the coated samples were measured before and after the testing to obtain the volume and weight loss. The volume loss of the pins were measured by the difference in length before and after. For coatings, the profilometer was used to measure the wear volume. To calculate the wear coefficient (k), Archard's equation was used.

$$k = \frac{Q}{W * L} \tag{3. 1}$$

In equation (3.1), Q is the total wear volume in mm^3, W is a load in newton (N), and L is the total sliding distance in meter (m).

CHAPTER 4 – RESULTS AND DISCUSSION

4.1 Structural characteristics of Ag-DLC coating on CoCrMo alloy

4.1.1 X-ray photoelectron spectroscopy analyses

X-ray photoelectron spectroscopy (XPS) was carried out on each sample. The XPS spectra were then analyzed using the Gaussian-Lorentzian function in CasaXPS software to obtain the chemical composition of the coatings. The chemical composition of the pure DLC coating and silver doped DLC coatings based on XPS are summarized in Table 4.1.

Table 4.1. Composition of coatings.

Coating	Oxygen (at.%)	Carbon (at.%)	Silver (at.%)
DLC	23.6	76.4	0
Ag-DLC-12W	38.8	60.8	0.4
Ag-DLC-14W	20.5	72.7	6.8
Ag-DLC-16W	15.9	76.6	7.4
Ag-DLC-18W	13.3	50.2	36.5

The silver's concentration increases as the power to the silver target increases from 12 W to 18 W. Oxygen is the most common contaminant for the coatings deposited in a moderate vacuum chamber and exposed to the atmosphere after deposition.

The contamination of oxygen creates C-O and C=O bonds inside the coating. The peaks for these oxides can be seen between 286 eV and 289 eV binding energy. The fine XPS spectrum of C1s peak for the DLC coating and its fitting curves are shown in Figure 4.1. The C1s peak can be deconvoluted into three peaks, sp^3 C-C peak at 284.6 eV, sp^2 C-C peak at 284

eV, and C-O peak at 286.23 eV. The peak at 284.6 eV shows much higher intensity than the peak at 284 eV, indicating higher sp^3 concentration in the DLC coating.

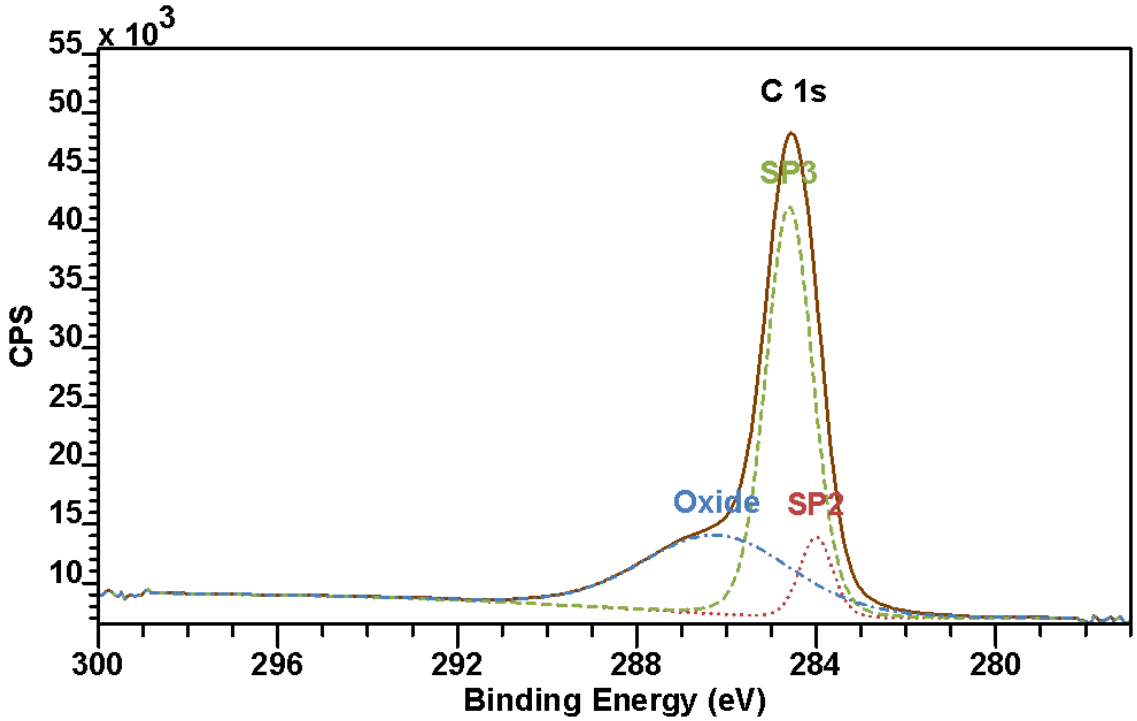

Figure 4.1. XPS C1s spectrum of DLC.

The fine XPS spectra of the C1s peak for the Ag-DLC coatings and their fitting curves are shown in Figure 4.2. As the silver concentration increases in the coating, the C1s peak moves towards a lower binding energy range and the peak intensity for sp^3 C-C bonds decreases, and the intensity for sp^2 C peak increases, showing that the doping of Ag decreases the sp^3 concentration of the DLC coatings and the higher the doping amount, the lower the sp^3 concentration. The binding energy of carbon in different chemical states in the coatings is listed in Table 4.2.

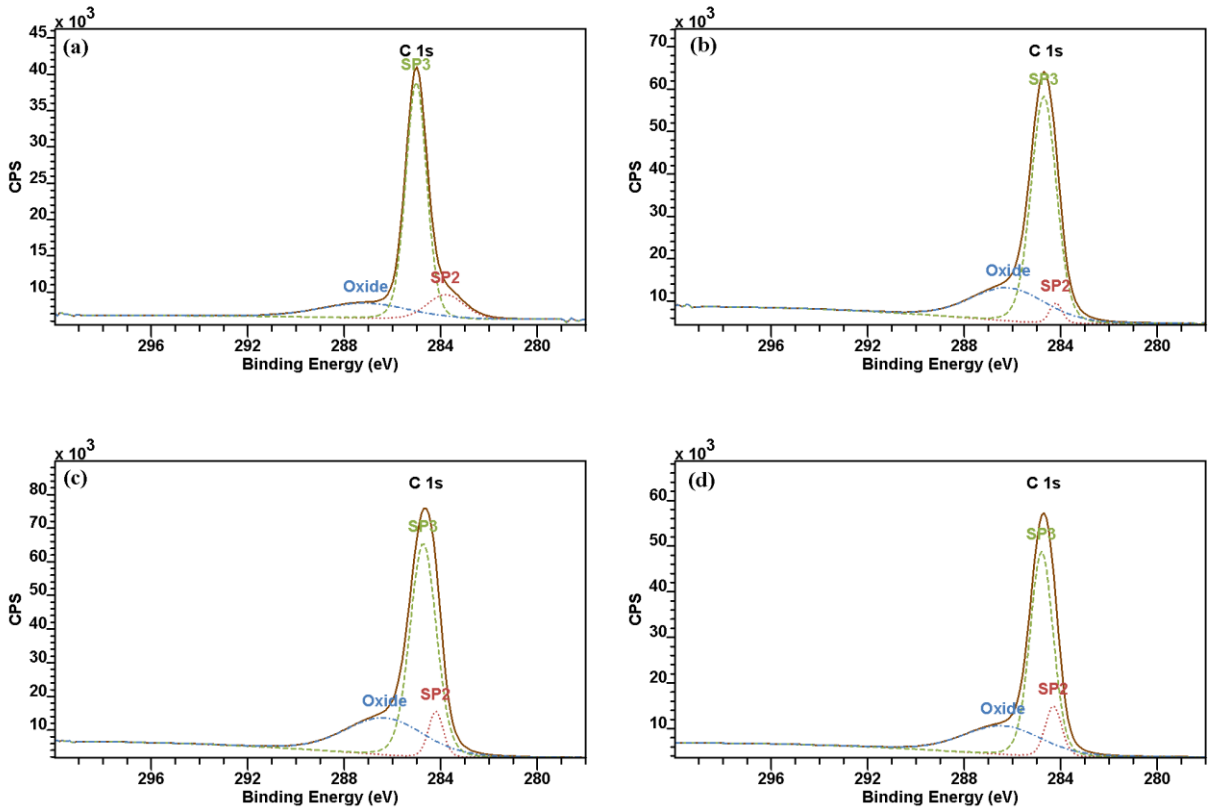

Figure 4.2. XPS C1s spectra of (a) Ag-DLC-12 W, (b) Ag-DLC-14 W, (c) Ag-DLC-16 W, and (d) Ag-DLC-18 W.

Table 4. 2 Binding energy of different chemical bonds in the coatings.

XPS Region	Coating	Chemical Bonds	Binding Energy (eV)
C1s	DLC	C-C (sp^3)	284.70
		C=C (sp^2)	284.00
		C-O, C=O	286.23
	Ag-DLC-12W	C-C (sp^3)	285.00
		C=C (sp^2)	283.90
		C-O, C=O	287.03
	Ag-DLC-14W	C-C (sp^3)	284.70
		C=C (sp^2)	284.10
		C-O, C=O	286.16
	Ag-DLC-16W	C-C (sp^3)	284.70
		C=C (sp^2)	284.10
		C-O, C=O	286.33
	Ag-DLC-18W	C-C (sp^3)	284.80
		C=C (sp^2)	284.30
		C-O, C=O	286.35

Figure 4.3 displays XPS images of the coatings, which show the distribution and the size of the silver particles in the carbon matrix. Origin graphical software was used to generate the images, and ImageJ software was used to analyze the size of the silver particles.

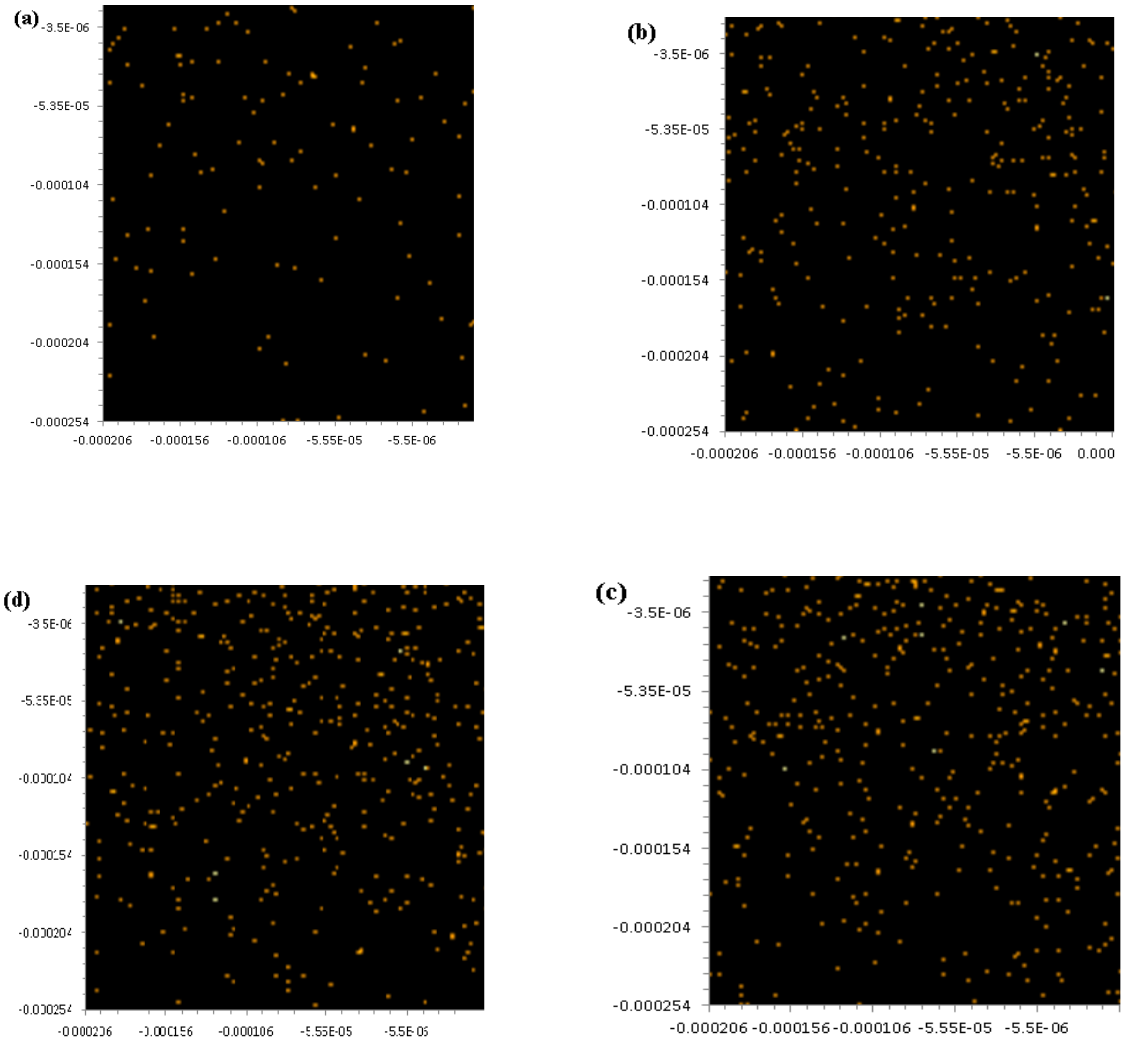

Figure 4.3. XPS mapping results of Ag in (a) Ag-DLC-12 W, (b) Ag-DLC-14 W, (c) Ag-DLC-16 W, and (d) Ag-DLC-18 W

As shown in Figure 4.3, the average silver particle density increases with the increase of silver concentration in the coatings. The average area of the silver particles in the coatings

measured using the ImageJ software is 253 nm^2, 341 nm^2, 379 nm^2, and 639 nm^2, respectively, for the samples with silver's concentration of 0.4 at.%, 6.8 at.%, 7.4 at.%, and 36.5 at.%, respectively. Mazare et al. [51] deposited Ag-DLC on titanium using a thermionic vacuum arc process and found that the particle size of silver increased with the increase of Ag concentration in the coating. A similar phenomenon was noticed by Wu et al. [50], and it was due to the tendency of Ag to form clusters on or near the surface during the deposition.

4.1.2 Raman spectroscopical analyses

The Raman spectra of DLC coating and silver doped DLC coatings are shown in Figure 4.4. As shown in Figure 4.4, two modes of carbon dominate the Raman spectra of the coatings. The graphite mode can be seen at the 1580 cm^{-1} labeled as 'G' and the disordered graphite mode at 1350 cm^{-1} labeled as 'D' [3]. The G mode of carbon, sp^2 bonds, is dominated in the Raman spectra because the π state has a lower energy level than the σ state of a carbon [3,27,28].

When the silver's concentration increases in the coating, the G peak moves towards a higher Raman shift. In comparison, the D peak moves oppositely towards the lower Raman shift. The intensity of the D peak increases, indicating the clustering of the sp^2 carbon and the chains type carbon bonding [31].

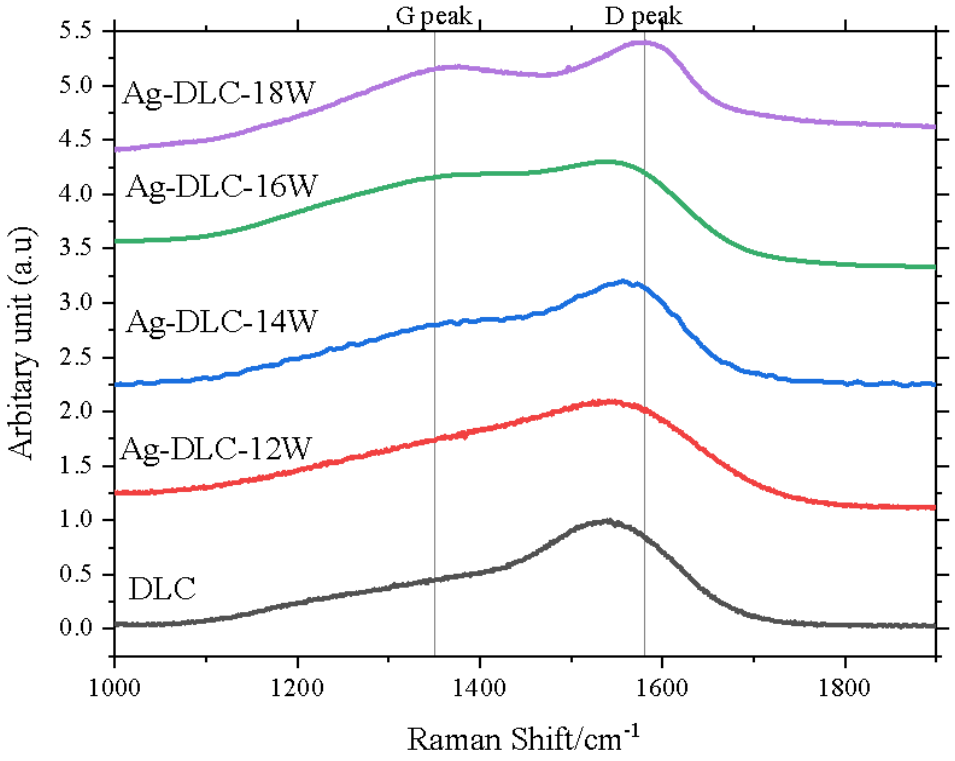

Figure 4.4. Raman spectra of DLC and Ag-DLC coatings.

The Raman spectra were fitted with Gaussian-Lorentzian function to the position of D and G peak and their intensity ratio, I(D)/I(G), as summarized in Table 4.3. The results show that the silver's incorporation into the carbon matrix increases the clustering of the sp^2 carbon because the intensity of the D peak is affected by the birthing vibrations of the aromatic rings [3,31,58]. Ferrari [31,58] found that the Raman spectrum of the disordered carbon can be described with a three-stage model. According to this model, the qualitative amount of the sp^3 carbon in the coating can be estimated based on the G peak position and the I(D)/I(G) ratio. The three-stage model of Ferrari is shown in Figure 4.5. Comparing the G peak and I(D)/I(G) ratio to the three-stage model, it can be noticed that the transformation of carbon bonds from sp^3 to sp^2 by Ag doping and the sp^2 content increases with the increase of Ag doping amount.

Table 4.3. The values of D peak, G peak and, I(D)/I(G) ratio.

Coating	D peak	G peak	I(D) / I(G)
DLC	1357	1546	0.80
Ag-DLC-12W	1367	1556	0.89
Ag-DLC-14W	1374	1558	0.95
Ag-DLC-16W	1399	1564	0.98
Ag-DLC-18W	1401	1583	1.34

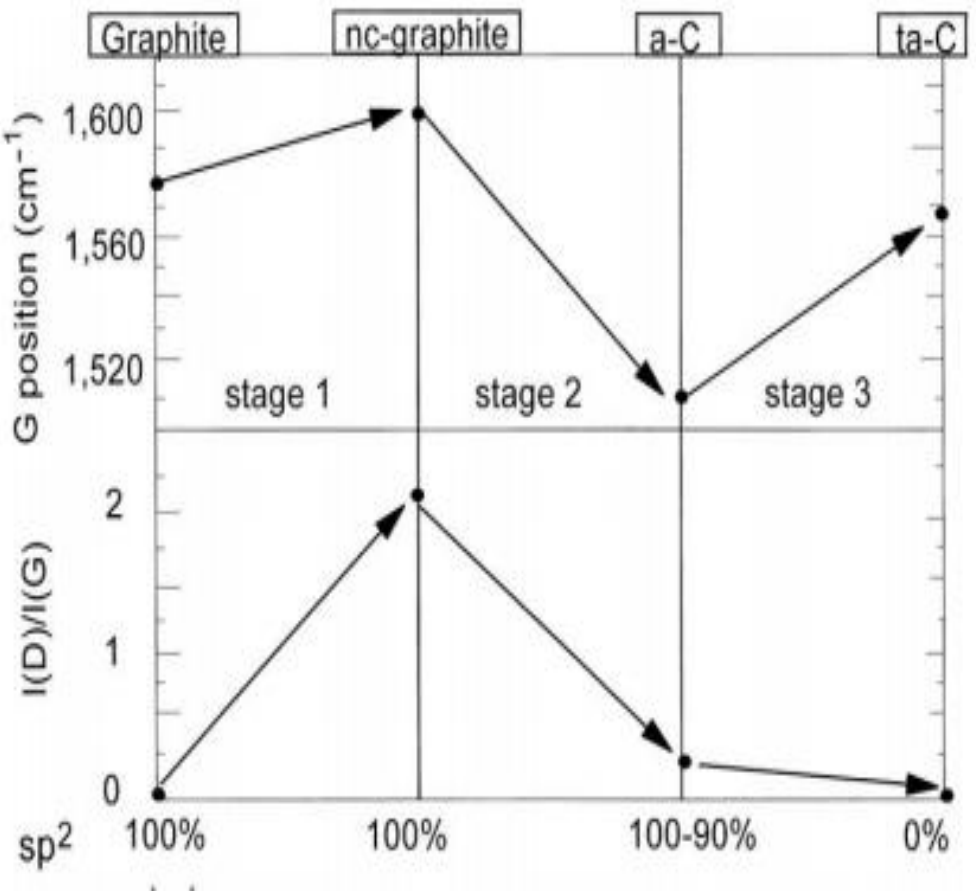

Figure 4.5. Three-stage model of amorphization of carbon.

4.2 Properties of Ag-DLC coating

4.2.1 Hardness and Young's Modulus

The hardness and Young's modulus of the thin coating samples are presented in Table 4.4. The DLC coating without doping shows the highest hardness of 24.1±1.2 GPa. The hardness decreases with the increase of Ag doping amount, and it is reduced to 20.1±1.1 GPa for a silver concentration of 7.4 at.%, and to 7.2±2.1 GPa for a silver's concentration of 36.5 at.%.

Table 4.4. Hardness and Young's modulus of Ag-DLC coatings.

Coating	Hardness (GPa)	Young's Modulus (GPa)	Thickness (μm)
DLC	24.1 ± 1.2	201.23 ± 5.21	1.40 ± 0.09
Ag-DLC-12W	22.8 ± 1.6	217.27 ± 9.37	1.74 ± 0.13
Ag-DLC-14W	21.7 ± 1.6	217.24 ± 13.84	2.12 ± 0.10
Ag-DLC-16W	20.1 ± 1.1	222.75 ± 12.12	2.20 ± 0.08
Ag-DLC-18W	7.2 ± 2.1	303.99 ± 64.03	2.70 ± 0.14

4.2.2 Adhesion and Internal Stress

The internal stress of the coating was measured using Stoney's equation (equation 4.1). Figure 4.6 shows the hardness and the internal stress of the coatings.

$$\sigma = \frac{E_s}{(1-v_s)} \times \frac{t_s^2}{6t_f}\left(\frac{1}{R_1} - \frac{1}{R_2}\right) \quad (4.1)$$

In equation 4.1, σ is the stress in the coating, E_s is elastic modulus of substrate, v_s is the Poisson's ratio of substrate, t_s and t_f are the thickness of substrate and coating, respectively, R_1 and R_2 are the radius of curvature before and after the coating, respectively.

As shown in Figure 4.6, the drop of the coating's compressive stress is huge due to Ag doping. On the contrary, the reduction in the hardness is not significant up to 7.4 at% doping. The drop of stress is probably due to the reduction of sp^3 carbon bonds and the formation of dispersed Ag particles in the coating.

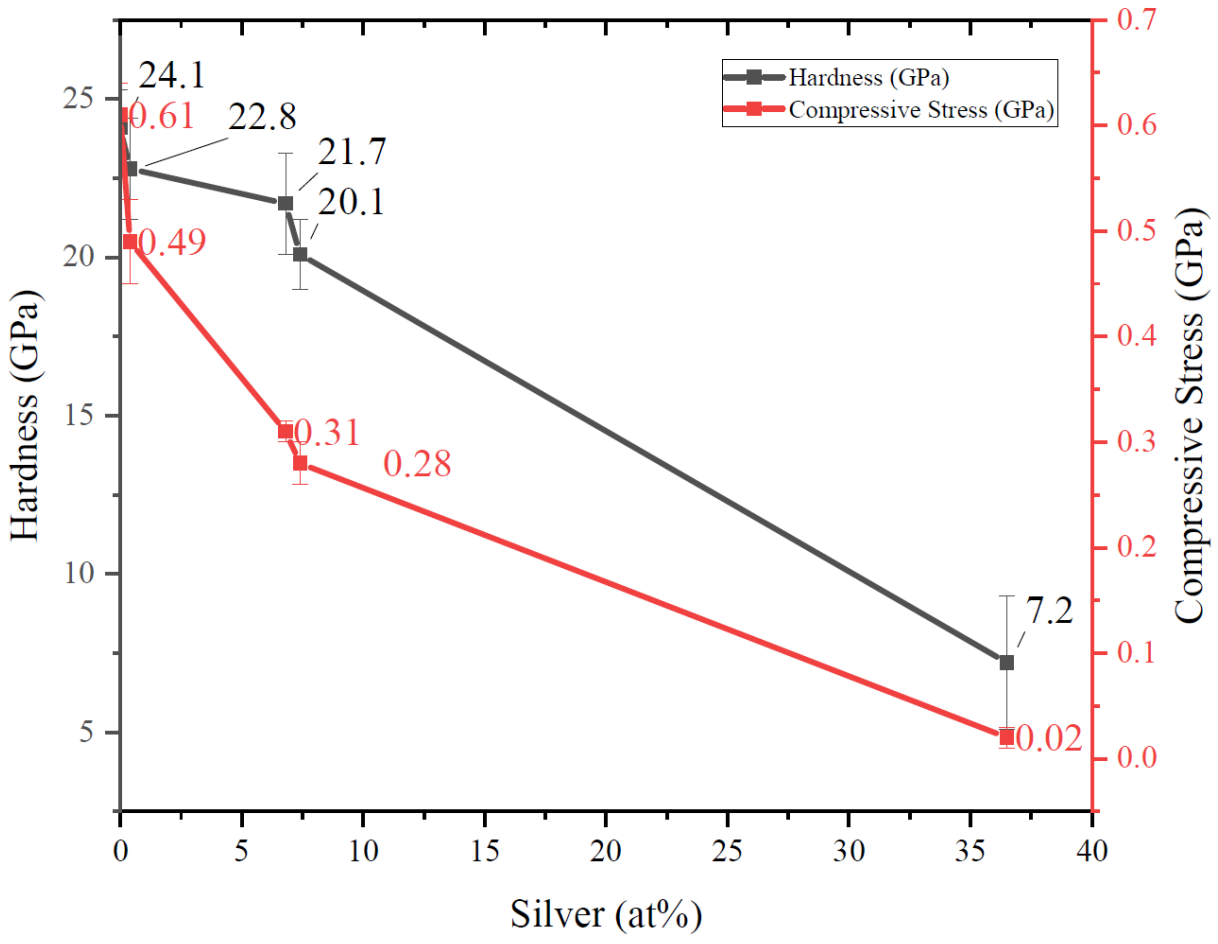

Figure 4.6. Hardness and the stress in the coating.

The compressive residual stress in the DLC coating is high due to the energetic deposition technique. The compressive stress is released by the coating's buckling, which occurs due to the coating-substrate interface's intrinsic defect. The remaining energy drives the coating's delamination [35]. How the residual stress in the DLC coating affects the adhesion has been described in section 2.3.2, which shows that the residual compressive stress would decrease the adhesion of the coatings

The SEM images of the indentation and its surrounding area after Rockwell C indentation testing are illustrated in Figure 4.7. As shown in the Figure 4.7, the adhesion of all silver doped DLC coating is acceptable according to the VDI 3198 indentation standard described in section 2.6.1. As the stress in the Ag-DLC-12W decreased from 0.61 GPa for pure DLC to below 0.49 GPa for Ag-doped samples, the coating's adhesion increased, and thus there were no cracks or delamination of the coating observed.

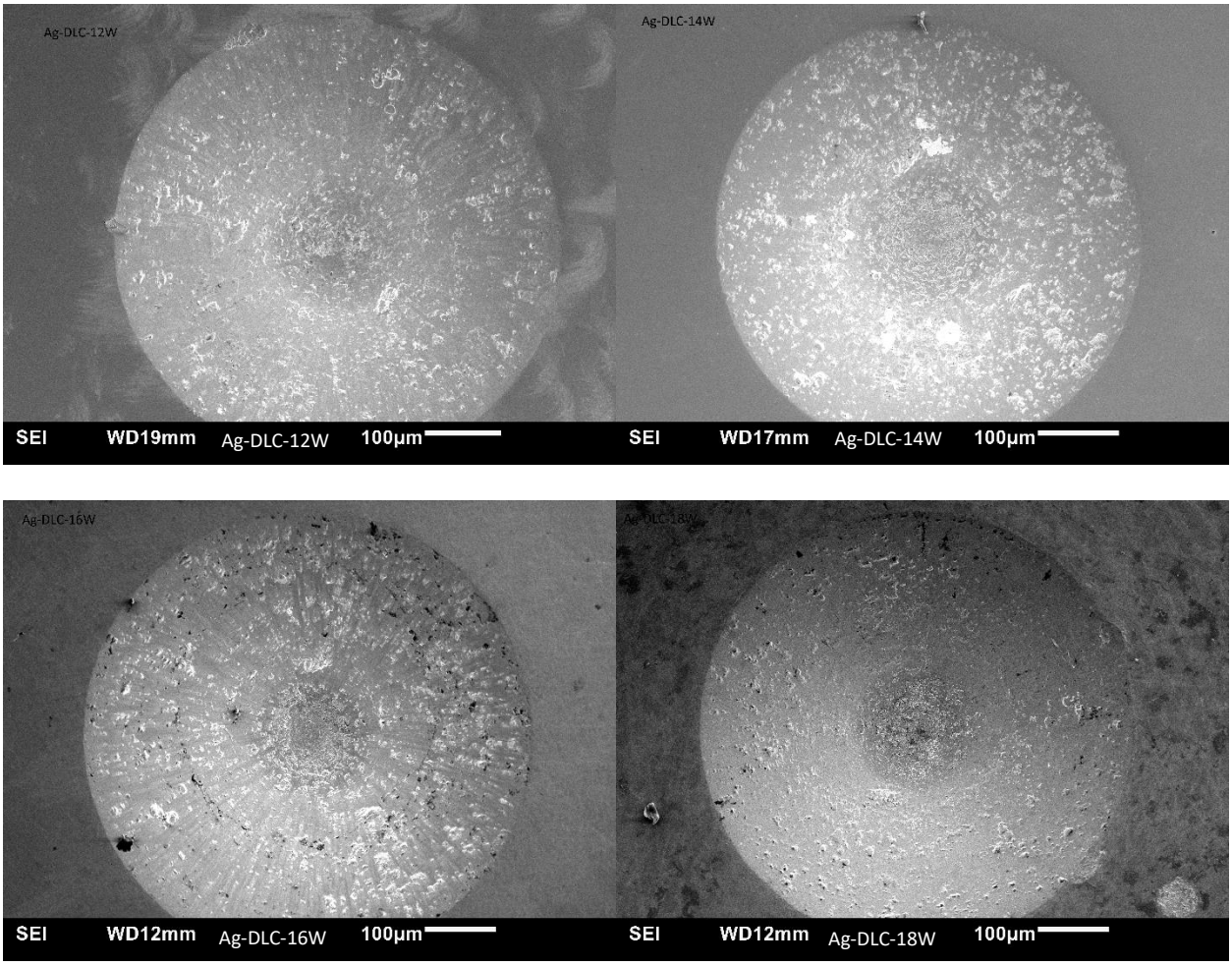

Figure 4.7. SEM images of Rockwell C indents on silver doped DLC coating.

4.2.3 Wear of Ag-DLC coating and UHMWPE

A pin-on-disk test was used to study the friction and the wear of the silver doped DLC coatings sliding with UHMWPE pins. After the testing, the volume loss of the coatings and the pins were measured. The results are summarized in Table 4.5.

Table 4.5. Volume loss and wear coefficient of Ag-DLC coating and UHMWPE.

Coating	Volume Loss of Coating (mm^3/10000 cycles)	Volume Loss of UHMWPE Pin (mm^3/10000 cycles)	Total Volume Loss (mm^3/10000 cycles)	Wear Coefficient (mm^3/N*m)
DLC	0.0000	3.1792	3.1792	0.001272
Ag-DLC-12W	0.0005	1.2717	1.2722	0.000509
Ag-DLC-14W	0.2025	0.9538	1.1563	0.000463
Ag-DLC-16W	0.3206	0.6358	0.9564	0.000383
Ag-DLC-18W	0.5344	0.4769	1.0113	0.000405

For DLC coating, the volume loss of the coating is significantly less, and the volume loss for the UHMWPE pin is very high, which resulted in a high total wear coefficient. As the silver's concentration increases in the coating from 0.4 at.% to 7.4 at.%, the volume loss of the coatings increases due to a drop in hardness, whereas the volume loss of the UHMWPE pins decreases, which resulted in the reduction of the total wear coefficient. But at the silver's concentration of 36.5 at.%, the combined volume loss increases due to the high volume loss of coating, which failed between 2000 to 4000 cycles. The images of the wear tracks are shown in Figure 4.8. The high wear rate of Ag-DLC-18W coating is probably due to its low hardness and high Ag concentration [36].

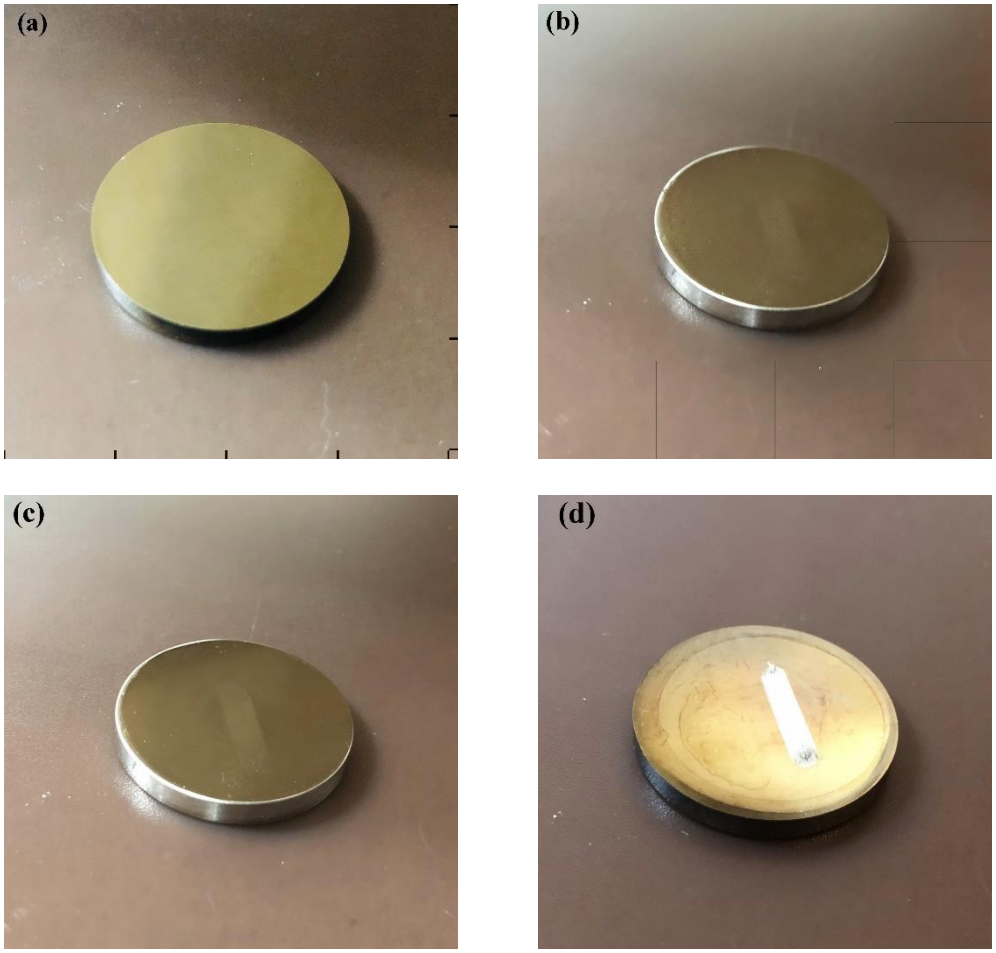

Figure 4.8. Wear tracks on (a) Ag-DLC-12 W, (b) Ag-DLC-14 W, (c) Ag-DLC-16 W, and (d) Ag-DLC-18 W.

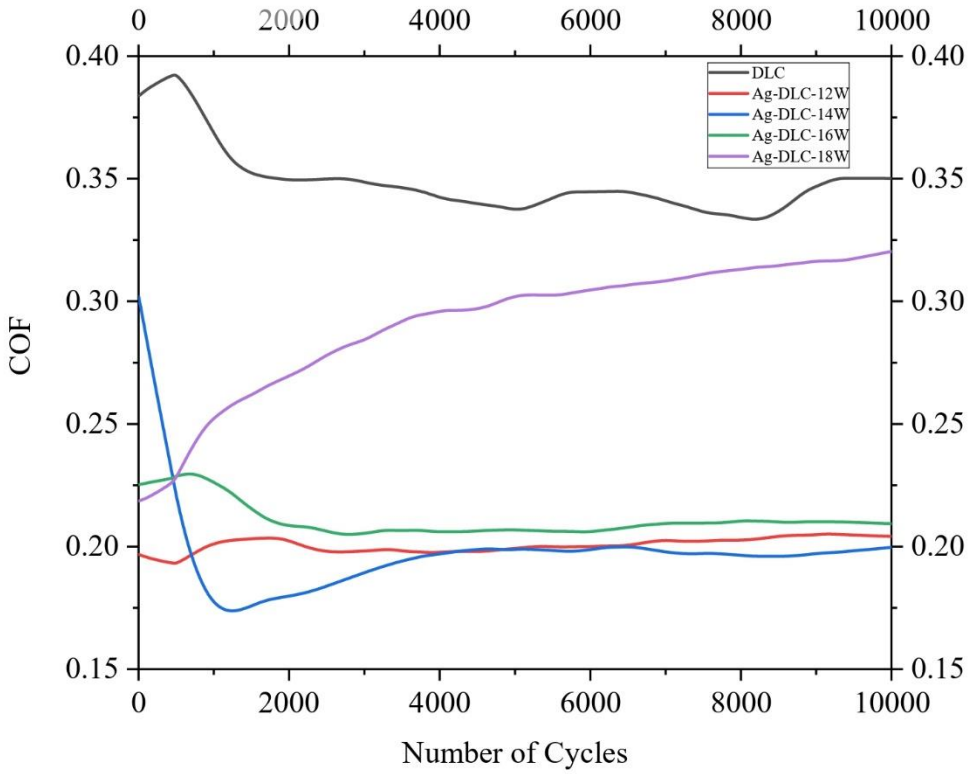

Figure 4.9. Coefficient of friction values for different coatings.

Figure 4.9 shows the graph of COF (coefficient of friction) vs. the number of cycles. The results show that Ag doping can significantly decrease the COF. For DLC coating, the friction coefficient ranges between 0.32 and 0.4, which is higher than that reported for DLC coatings [42,49,59]. DLC coating's low friction coefficient is usually due to the formation of the transfer layer on the counterpart [53]. However, in the present DLC vs. UHMWPE pin case, the pin's wear loss is very high, which may prevent the formation of a transfer layer.

For Ag-DLC with silver’s concentration of 0.4 at.% to 7.4 at.%, the friction coefficient is between 0.18 and 0.22 after 2000 cycles, much lower than that of pure DLC, which is probably due to the formation of a solid lubricant layer of Ag between the coating and the UHMWPE pin.

CHAPTER 5 – CONCLUSIONS AND RECOMMENDATIONS FOR FUTURE WORK

5.1 Summary and Conclusions

Silver doped DLC coatings with Ag concentration from 0.4 at.% to 36.5 at.% were successfully deposited on CoCrMo alloy using magnetron sputtering, and their mechanical and tribological properties were characterized. The main results and conclusions are summarised as follows.

1. Ag doping reduces sp^3 carbon in the coatings, and the higher the Ag concentration, the lower the sp^3 carbon concentration. Consequently, the compressive residual stress in the coatings decreases from 0.61 GPa for 0% Ag to 0.02 GPa for 36.5 at.% Ag.
2. As Ag doping decreases sp^3 carbon concentration in the coatings, coating hardness decreases, and adhesion increases with the increase of Ag doping concentration.
3. When doping with 7.4 at.% Ag, the residual internal stress reduces by 54.1%, whereas the hardness only decreases by 16.6%, indicating doping low amount Ag can maintain high hardness but significantly reduce residual stress.
4. When sliding with UHMWPE, pure DLC coating shows high friction coefficient and a very high wear rate of UHMWPE. Low amount Ag doping up to 7.4 at.% reduces friction coefficient and decreases the wear rate of UHMWPE, and total wear coefficient decreases. But for a high amount of Ag doping, the total wear coefficient increases due to the high wear rate of the highly doped DLC coating.

5.2 Recommendations for Future Work

Previous research showed that for biomedical applications, the concentration of silver should be limited to 10 at.%, but the present study shows that DLC coatings doped with 5 at.%

to 10 at.% would be of most interest. Therefore, further systematic research on the process parameters is suggested to obtain DLC coating with 5 at.% to 10 at.% Ag doping for better-combined wear resistance. In addition, the following tests are also recommended:

1. Since silver shows very good antibacterial properties, which is desirable for joint applications, antibacterial tests on Ag-doped coatings are recommended to be performed to understand their antibacterial performance.
2. For tribological properties, it is recommended to do testing under simulated hip joint conditions.
3. It is also recommended to do tribo-corrosion and ion release testing under simulated joint conditions.

REFERENCES

[1] S. Kurtz, K. Ong, E. Lau, F. Mowat, M. Halpern, Projections of primary and revision hip and knee arthroplasty in the United States from 2005 to 2030, JBJS. 89 (2007) 780–785. https://journals.lww.com/jbjsjournal/Fulltext/2007/04000/Projections_of_Primary_and_Revision_Hip_and_Knee.12.aspx.

[2] M. Geetha, A.K. Singh, R. Asokamani, A.K. Gogia, Ti based biomaterials, the ultimate choice for orthopaedic implants – A review, Prog. Mater. Sci. 54 (2009) 397–425. doi:10.1016/J.PMATSCI.2008.06.004.

[3] J. Robertson, Diamond-like amorphous carbon, Mater. Sci. Eng. R Reports. 37 (2002) 129–281. doi:10.1016/s0927-796x(02)00005-0.

[4] D. Batory, M.C. Reczulska, L. Kolodziejczyk, W. Szymanski, Gradient titanium and silver based carbon coatings deposited on AISI316L, Appl. Surf. Sci. 275 (2013) 303–310. doi:10.1016/j.apsusc.2012.12.088.

[5] P. Písařík, M. Jelínek, J. Remsa, J. Mikšovský, J. Zemek, K. Jurek, Kubinová, J. Lukeš, J. Šepitka, Antibacterial, mechanical and surface properties of Ag-DLC films prepared by dual PLD for medical applications, Mater. Sci. Eng. C. 77 (2017) 955–962. doi:10.1016/j.msec.2017.04.005.

[6] L. Swiatek, A. Olejnik, J. Grabarczyk, A. Jedrzejczak, A. Sobczyk-Guzenda, M. Kaminska, W. Jakubowski, W. Szymanski, D. Bociaga, Multi-doped diamond like-carbon coatings (DLC-Si/Ag) for biomedical applications fabricated using the modified chemical vapour deposition method, Diam. Relat. Mater. 67 (2016) 54–62. doi:10.1016/j.diamond.2016.03.005.

[7] I. Carvalho, M. Curado, C. Palacio, S. Carvalho, A. Cavaleiro, Ag release from sputtered Ag/a:C nanocomposite films after immersion in pure water and NaCl solution, Thin Solid Films. 671 (2019) 85–94. doi:10.1016/j.tsf.2018.12.010.

[8] A. Tyagi, R.S. Walia, Q. Murtaza, S.M. Pandey, P.K. Tyagi, B. Bajaj, A critical review of diamond like carbon coating for wear resistance applications, Int. J. Refract. Met. Hard Mater. 78 (2019) 107–122. doi:10.1016/j.ijrmhm.2018.09.006.

[9] J.K.J.R. Maguire, M.F. Coscia, M.H. Lynch, Foreign body reaction to polymeric debris following total hip arthroplasty, A Publ. Assoc. Bone Jt. Surg. | CORR®. 216 (1987). https://journals.lww.com/clinorthop/Fulltext/1987/03000/Foreign_Body_Rea

ction_to_Polymeric_Debris.35.aspx.

[10] M. Merola, S. Affatato, Materials for hip prostheses : A review of wear and loading considerations, Mater. 12 (2019) 495. doi:10.3390/ma12030495.

[11] S. Affatato, F. Traina, O. Ruggeri, A. Toni, Wear of metal-on-metal hip bearings: metallurgical considerations after hip simulator studies, Int. J. Artif. Organs. 34 (2011) 1155–1164. doi:10.5301/ijao.5000065.

[12] A.S.M. International, ASM Specialty Handbook: Nickel, Cobalt, and Their Alloys (#06178G), 2000.

[13] G.W. (Gwidon W.. Stachowiak, A.W. (Andrew W.. Batchelor, Contact between two elastic spherical or spheroidial bodies, in: Eng. Tribol., 2005.

[14] D. Hu, K. Tie, X. Yang, Y. Tan, M. Alaidaros, L. Chen, Comparison of ceramic-on-ceramic to metal-on-polyethylene bearing surfaces in total hip arthroplasty: a meta-analysis of randomized controlled trials, J. Orthop. Surg. Res. 10 (2015) 22. doi:10.1186/s13018-015-0163-2.

[15] US FDA, Biological Responses to Metal Implants, Food Drug Admistration. (2019) 1–143.

[16] hip-replacement.jpg (1500×825), (n.d.). https://healthjade.com/wp-content/uploads/2018/06/hip-replacement.jpg (accessed April 10, 2021).

[17] J.C. Sánchez-López, A. Fernández, Doping and Alloying Effects on DLC Coatings, in: Tribol. Diamond-Like Carbon Film., Springer US, Boston, MA, 2008: pp. 311–338. doi:10.1007/978-0-387-49891-1_12.

[18] E. Haynes, Metal Alloy, 1907. https://patentimages.storage.googleapis.com/c0/76/60/5e006f0dacd6ff/US873745.pdf (accessed March 26, 2021).

[19] E. Bettini, C. Leygraf, J. Pan, Nature of current increase for a CoCrMo alloy: “transpassive” dissolution vs. water oxidation, Int. J. Electrochem. Sci. (2013).

[20] Standard Specification for Cobalt-28 Chromium-6 Molybdenum Alloy Castings and Casting Alloy for Surgical Implants (UNS R30075) 1, Annu. B. ASTM Stand. (2007) 7–10. doi:10.1520/F0075-07.2.

[21] B.M. Wroblewski, P.A. Fleming, P.D. Siney, Charnley low-frictional torque arthroplasty of the hip, J. Bone Jt. Surg. - Ser. B. (1999). doi:10.1302/0301-620X.81B3.9521.

[22] ASTM International (D6712-17), Standard specification for ultra-high-molecular-weight polyethylene (UHMW-PE) solid plastic shapes, 08.03 (2020) 1–4. doi:10.1520/D6712-17.2.

[23] N.A. Campbell, Campbell biology 10th Edition, 2013. doi:10.1017/CBO9781107415324.004.

[24] The nature of the chemical bond and the structure of molecules and crystals, Nature. 148 (1941) 677. doi:10.1038/148677c0.

[25] R. Hauert, DLC films in biomedical applications, in: Tribol. Diamond-Like Carbon Film. Fundam. Appl., 2008: pp. 494–509. doi:10.1007/978-0-387-49891-1_20.

[26] S. Aisenberg, R. Chabot, Ion-beam deposition of thin films of diamondlike carbon, J. Appl. Phys. 42 (1971) 2953–2958. doi:10.1063/1.1660654.

[27] J. Robertson, Diamond-like carbon, Pure Appl. Chem. 66 (1994) 1789–1796. doi:10.1351/pac199466091789.

[28] J. Robertson, Deposition mechanisms for promoting sp3 bonding in diamond-like carbon, Diam. Relat. Mater. 2 (1993) 984–989. doi:10.1016/0925-9635(93)90262-Z.

[29] J. Schwan, S. Ulrich, H. Roth, H. Ehrhardt, S.R.P. Silva, J. Robertson, R. Samlenski, R. Brenn, Tetrahedral amorphous carbon films prepared by magnetron sputtering and dc ion plating, J. Appl. Phys. 79 (1996) 1416–1422. doi:10.1063/1.360979.

[30] J.E. Greene, Review Article: Tracing the recorded history of thin-film sputter deposition: From the 1800s to 2017, J. Vac. Sci. Technol. A Vacuum, Surfaces, Film. 35 (2017) 05C204. doi:10.1116/1.4998940.

[31] W.I. Milne, Tetrahedrally bonded amorphous carbon, in: J. Non. Cryst. Solids, 1996: pp. 605–610. doi:10.1016/0022-3093(95)00773-3.

[32] E.G. Spencer, P.H. Schmidt, D.C. Joy, F.J. Sansalone, Ion-beam-deposited polycrystalline diamondlike films, Appl. Phys. Lett. 29 (1976) 118–120. doi:10.1063/1.88963.

[33] Y. Lifshitz, S.R. Kasi, J.W. Rabalais, W. Eckstein, Subplantation model for film growth from hyperthermal species, Phys. Rev. B. 41 (1990) 10468–10480. doi:10.1103/PhysRevB.41.10468.

[34] J.E. Inglesfield, Physics of graphite, Phys. Bull. 33 (1982) 333–333. doi:10.1088/0031-9112/33/9/037.

[35] Y. Pauleau, Residual Stresses in DLC Films and Adhesion to Various Substrates, in: Tribol. Diamond-Like Carbon Film., Springer US, Boston, MA, 2008: pp. 102–136. doi:10.1007/978-0-387-49891-1_4.

[36] J. Fontaine, C. Donnet, A. Erdemir, Fundamentals of the tribology of DLC coatings, Tribol. Diamond-Like Carbon Film. Fundam. Appl. (2008) 139–154. doi:10.1007/978-0-387-49891-1_5.

[37] V.M. Tiainen, Amorphous carbon as a bio-mechanical coating-mechanical properties and biological applications, Diam. Relat. Mater. 10 (2001) 153–160. doi:10.1016/S0925-9635(00)00462-3.

[38] R. Lappalainen, H. Heinonen, A. Anttila, S. Santavirta, Some relevant issues related to the use of amorphous diamond coatings for medical applications, Diam. Relat. Mater. 7 (1998) 482–485. doi:10.1016/s0925-9635(98)80003-4.

[39] J.I. Oate, M. Comin, I. Braceras, A. Garcia, J.L. Viviente, M. Brizuela, N. Garagorri, J.L. Peris, J.I. Alava, Wear reduction effect on ultra-high-molecular-weight polyethylene by application of hard coatings and ion implanation on cobalt chromium ally, as measured in a knee wear simulation machine, Surf. Coatings Technol. 142–144 (2001) 1056–1062. doi:10.1016/S0257-8972(01)01074-X.

[40] D. Ugolini, J. Eitle, P. Oelhafen, Influence of process gas and deposition energy on the atomic and electronic structure of diamond-like (a-C:H) films, Vacuum. 41 (1990) 1374–1377. doi:10.1016/0042-207X(90)93961-H.

[41] M. Wang, K. Schmidt, K. Reichelt, H. Dimigen, H. Hübsch, The properties of titanium-containing amorphous hydrogenated carbon films, Surf. Coatings Technol. 47 (1991) 691–695. doi:10.1016/0257-8972(91)90342-T.

[42] L. Kolodziejczyk, W. Szymanski, D. Batory, A. Jedrzejczak, Nanotribology of silver and silicon doped carbon coatings, Diam. Relat. Mater. 67 (2016) 8–15. doi:10.1016/j.diamond.2015.12.010.

[43] M. Chhowalla, Thick, well-adhered, highly stressed tetrahedral amorphous carbon, Diam. Relat. Mater. 10 (2001) 1011–1016. doi:10.1016/S0925-9635(00)00530-6.

[44] J.-P. Hirvonen, J. Koskinen, J.R. Jervis, M. Nastasi, Present progress in the development of low friction coatings, Surf. Coatings Technol. 80 (1996) 139–150. doi:10.1016/0257-8972(95)02701-7.

[45] K. Oguri, T. Arai, Friction coefficient of SiC, TiC and GeC coatings with excess carbon formed by plasma-assisted chemical vapour deposition, Thin

Solid Films. 208 (1992) 158–160. doi:10.1016/0040-6090(92)90635-O.

[46] K. Oguri, T. Arai, Effect of excess carbon on the hardness of SiC and TiC coatings formed by plasma-assisted chemical vapor deposition, Thin Solid Films. 186 (1990) L29–L31. doi:10.1016/0040-6090(90)90152-4.

[47] R. Memming, H.J. Tolle, P.E. Wierenga, Properties of polymeric layers of hydrogenated amorphous carbon produced by a plasma-activated chemical vapour deposition process II: Tribological and mechanical properties, Thin Solid Films. 143 (1986) 31–41. doi:10.1016/0040-6090(86)90144-6.

[48] I. Karakaya, W.. Thompson, Ag-C Phase diagram, Bull. Alloy Phase Dia. 9 (1988) 282–284.

[49] N.K. Manninen, F. Ribeiro, A. Escudeiro, T. Polcar, S. Carvalho, A. Cavaleiro, Influence of Ag content on mechanical and tribological behavior of DLC coatings, Surf. Coatings Technol. 232 (2013) 440–446. doi:10.1016/j.surfcoat.2013.05.048.

[50] Y. Wu, J. Chen, H. Li, L. Ji, Y. Ye, H. Zhou, Preparation and properties of Ag/DLC nanocomposite films fabricated by unbalanced magnetron sputtering, Appl. Surf. Sci. 284 (2013) 165–170. doi:10.1016/j.apsusc.2013.07.074.

[51] A. Mazare, A. Anghel, C. Surdu-Bob, G. Totea, I. Demetrescu, D. Ionita, Silver doped diamond-like carbon antibacterial and corrosion resistance coatings on titanium, Thin Solid Films. 657 (2018) 16–23. doi:10.1016/j.tsf.2018.04.036.

[52] K. Baba, R. Hatada, S. Flege, W. Ensinger, Y. Shibata, J. Nakashima, T. Sawase, T. Morimura, Preparation and antibacterial properties of Ag-containing diamond-like carbon films prepared by a combination of magnetron sputtering and plasma source ion implantation, Vacuum. 89 (2013) 179–184. doi:10.1016/j.vacuum.2012.04.015.

[53] C. Donnet, A. Erdemir, Tribology of diamond-like carbon films, Springer US, Boston, MA, 2008. doi:10.1007/978-0-387-49891-1.

[54] A. Ferrari, J. Robertson, Interpretation of Raman spectra of disordered and amorphous carbon, Phys. Rev. B - Condens. Matter Mater. Phys. 61 (2000) 14095–14107. doi:10.1103/PhysRevB.61.14095.

[55] P. van der Heide, X-Ray photoelectron spectroscopy, John Wiley & Sons, Inc., Hoboken, NJ, USA, 2011. doi:10.1002/9781118162897.

[56] N. Vidakis, A. Antoniadis, N. Bilalis, The VDI 3198 indentation test evaluation of a reliable qualitative control for layered compounds, J. Mater. Process. Technol. 143–144 (2003) 481–485. doi:10.1016/S0924-0136(03)00300-5.

[57] BSI Standards Publication Metallic materials — Instrumented indentation test of hardness and materials parameters Part 1 : Test method, (2015).

[58] A.C. Ferrari, J. Robertson, M.G. Beghi, C.E. Bottani, R. Ferulano, R. Pastorelli, Elastic constants of tetrahedral amorphous carbon films by surface Brillouin scattering, Appl. Phys. Lett. 75 (1999) 1893–1895. doi:10.1063/1.124863.

[59] G. Fiaschi, A. Rota, A. Ballestrazzi, D. Marchetto, E. Vezzalini, S. Valeri, A Chemical, Mechanical, and Tribological Analysis of DLC Coatings Deposited by Magnetron Sputtering, Lubricants. 7 (2019) 38. doi:10.3390/lubricants7040038.